AIRS
Atmospheric Infrared Sounder

Algorithm Theoretical Basis Document

Level 1B

Part 1: Infrared Spectrometer

Version 8.0

H. H. Aumann, Evan Manning, Thomas Pagano, Steven Broberg, Robert Wilson, Steve Licata, Igor Yanovsky

Jet Propulsion Laboratory
California Institute of Technology
Pasadena, California

Ken Overoye
Formerly BAE Systems, Nashua, New Hampshire, 03064

15, June, 2024

JPL URS325639

The research was carried out at the Jet Propulsion Laboratory, California Institute of Technology, under a contract with the National Aeronautics and Space Administration.

Table of Contents

Release History:

The version number of the Level 1B ATBD is synchronized with the PGE version, which is used for routine data processing at the GES DISC and at NOAA/NESDIS.

Version 1.0 November 18, 2000 pre-launch calibration

Version 2.0 Not released. No significant changes

Version 3.0 Not released. No significant changes

Version 4.0 First official post-launch release of the Level 1B ATBD

a) Handling of space views.
b) Handling of radiation-hit-induced spikes in the observed signal from the on-board calibrator;
c) Handling and flagging detectors with significant non-Gaussian noise (cold scene noise, popping, and radiation hits);

Version 5.0 Produced routinely since August 31, 2002.

Format changes to EOS-HDF

No change in the calibrated radiances (uses the prelaunch calibration coefficient)

Version 6.0 Internal version.

No change to the calibrated radiances

Improved spectra calibration for each data granule.

Version 7.0 Internal version

Format change to Net CDF

First adjustment of the radiometric calibration since launch

includes on-orbit tests results in the calibration

includes a scan angle and time dependent polarization

includes a time dependent change in the polarization coefficients

includes A/B separate nonlinearity coefficients

Version V8. First version with post-launch calibration coefficients and updated spectral calibration.

1. Introduction

The AIRS Infrared Level 1B Algorithm Theoretical Basis Document (ATBD) describes the theoretical basis of the algorithms used to convert the output of the Atmospheric Infrared Sounder (AIRS) from engineering units to physical radiance units, to evaluate the positions of the Spectral Response Function (SRF) and provide estimates of the noise for all 2378 spectral channels. The description of the algorithms that convert the Level 1B measurements to geophysical quantities is covered in the Level 2 ATBD.

There are many papers and reports related to the Level 1B ATBD: An overall description of the AIRS instrument development is given in Ref. 1. The AIRS Functional Requirements Document (FRD) is in Ref. 2. The AIRS Calibration Plan, Ref. 3, contains a description of the relevant parts of the AIRS instrument, calibration devices and calibration procedures for pre-launch and in-orbit characterization of parameters needed by the Level 1B algorithms. The AIRS Validation Plan, Ref. 4, describes post-launch validation of Level 1B data using floating buoys, radiosondes, and satellite- and aircraft-borne instruments. The AIRS Version 8 Test Report (Ref. 5) provides comprehensive testing of the V8 data product and QC and compares results with the V5 L1B data product.

2. Instrument Overview

The Atmospheric Infrared Sounder is a high spectral resolution IR spectrometer. AIRS, together with the Advanced Microwave Sounding Unit (AMSU) and the Microwave Humidity Sounder supplied by Brazil (HSB), is designed to meet the operational weather prediction requirements of the National Oceanic and Atmospheric Administration (NOAA) and the global change research objectives of the National Aeronautics and Space Administration (NASA). The AIRS flight model calibration started in November 1998 and was completed in November 1999. Integration onto the spacecraft was completed in January 2001. Aqua, the EOS spacecraft carrying the three instruments, was launched from Vandenberg AFB on May 4, 2002. Details of the science objectives are found in Ref. 6.

The AIRS instrument includes an infrared spectrometer and a visible light/near-infrared photometer. The infrared portion of AIRS is a pupil-imaging infrared grating spectrometer with spectral coverage from 3.74 to 4.61 μm, from 6.20 to 8.22 μm, and from 8.8 to 15.4 μm. The nominal spectral resolution, $\lambda/\Delta\lambda$, is 1200, but it varies as a function of frequency from 1080 to nearly 1600. The spectrum is sampled twice per spectral resolution element for a total of 2378 spectral samples. The diffraction grating disperses the radiation onto 17 linear arrays of HgCdTe detectors in grating orders 3 through 11. Because of the modular nature of the linear arrays and optical system, the calibration coefficients show a modular dependence. A list of the 17 modules, their names and wavenumber and wavelength coverage is shown in Table 2-1.

The position of the dispersed beam on the focal plane in the dispersed and in the cross-dispersed direction can be accurately controlled by pivoting the collimation mirror using the Actuator Mirror Assembly (AMA). The AMA proved to be critical during the pre-launch calibration, but has not been needed in orbit to date.

The scan head assembly contains the scan mirror and calibrators. The scan mirror rotates through 360 degrees every 2.667 seconds. This produces data for one scan line with 90 footprints on the ground and

Table 2-1. Channel ID Spectral Range of Centroids in the AIRS 17 Modules.

Module	Name	Channel Start	Channel Stop	Wavenumber (cm^{-1})	Wavenumber (cm^{-1})	Wavelength (μm)	Wavelength (μm)
1	M1a	2261	2378	2541.90	2665.24	3.93407	3.75200
2	M1b	2015	2144	2299.80	2422.85	4.34821	4.12737
3	M2a	2145	2260	2446.19	2569.75	4.08798	3.89143
4	M2b	1865	2014	2181.49	2325.06	4.58401	4.30096
5	M3	1463	1654	1338.16	1443.07	7.47294	6.92965
6	M4a	1761	1864	1541.10	1613.86	6.48889	6.19632
7	M4b	1655	1760	1460.27	1527.00	6.84807	6.54877
8	M4c	1369	1462	1284.35	1338.86	7.78605	7.46902
9	M4d	1263	1368	1216.97	1272.59	8.21710	7.85800
10	M5	1104	1262	1056.08	1136.63	9.46902	8.79791
11	M6	937	1103	973.818	1046.20	10.2689	9.55844
12	M7	770	936	911.235	974.294	10.9741	10.2638
13	M8	609	769	851.490	903.777	11.7441	11.0646
14	M9	442	608	789.263	852.425	12.6700	11.7312
15	M10	275	441	728.055	781.882	13.7352	12.7896
16	M11	131	274	687.601	728.439	14.5433	13.7279
17	M12	1	130	649.620	681.993	15.3936	14.6629

6 calibration-related footprints. The scan mirror motor operates in two speed regimes. During the first 2 seconds it rotates at 49.5 degrees/second to generate a scan line with 90 ground footprints, each with a 1.1 degree diameter FOV. During the final 0.667 seconds, the scan mirror finishes the remaining 261 degrees of a full revolution. Routine calibration-related data is acquired during this time. These consist of four independent Cold Space Views (CSVs), one view into the Onboard Radiometric Calibrator (OBC), one view into the Onboard Spectral Reference Source (OBS), and one view into a photometric calibrator for the VIS/NIR photometer.

The IR spectrometer is cooled by a two-stage radiative cooler. The temperature of the spectrometer is monitored with six fully redundant temperature sensors. It is fine-controlled by a temperature servo in combination with a 2.8-watt heater. The temperature can be set to within 0.008 K. The servo heater can raise the spectrometer temperature set point by a maximum of 7 degrees above the natural orbital conditions, observed to be between 150 K and 165 K. Since January 2004 the operating temperature of the spectrometer is set to 155.56 K. Full radiometric and spectral calibrations were conducted prelaunch in the AIRS Test and Calibration Facility (ATCF) at spectrometer temperatures of 149 K, 155 K and 161 K. These measurements show excellent radiometric and spectral calibration stability. The measurements also have confirmed the 20-hour thermal time constant of the spectrometer.

The scan mirror is cooled by radiative coupling to the cold IR spectrometer, resulting in a mirror temperature approximately 40 K cooler than the spacecraft ambient temperature of 296 K, but 100 K

warmer than the spectrometer temperature. The scan mirror temperature is monitored by a non-contact sensor located at the base of the rotating shaft, about 6 inches from the scan mirror surface. The temperature difference between the scan mirror surface and the temperature sensor is estimated to be less than 0.5 K. Temperature variations across the scan mirror surface are less than 0.05 K peak-to-peak. The scan mirror is coated with silver and overcoated with a protective layer of SiO_2 by Denton using a proprietary process. The scan mirror temperature, mirror angle (relative to nadir), emissivity and polarization are components of the radiometric calibration algorithm.

2.1. On-board Calibration Devices

Routine IR radiometric calibration related data are taken while the scan mirror rotates from +49.5 degrees (relative to nadir) through 180 degrees (anti-nadir position) to -49.5 degrees. These data consist of four independent views of cold space (CSV) and one view into the Onboard Radiometric Calibrator (OBC) source. The view into the Onboard Spectral Reference Source (OBS) once per scan line was used as a check of the spectral calibration during pre-launch testing. In-orbit, the upwelling spectral radiance from the nadir footprints is used for the spectral calibration. The AIRS spectrometer is pupil imaging, i.e. detectors are located at a pupil stop of the spectrometer optics, as opposed to the detectors being at a field stop, i.e. imaging the scene on the detectors. This ensures that radiometric impacts due to spatial non-uniformity in the on-board calibration targets and the scene are minimized.

2.1.1. Onboard Radiometric Calibrator (OBC)

The OBC is a deep wedge cavity blackbody with a rectangular, clear aperture 5.7 cm by 9.5 cm. The depth of the blackbody cavity is twice the diagonal of the clear aperture. The blackbody housing and cavity are made from beryllium to reduce its mass to 2 kg. The surface of the OBC wedge cavity is coated with paint with emissivity higher than 0.91. Considering multiple reflections inside the wedge, the OBC effective emissivity is calculated to be greater than 0.99994 (Ref 6).

Four semi-conductor resistance temperature sensors, T1–T4, monitor the temperature at key positions to an accuracy of 0.1 K. T1 and T2 are located on the sloping part of the wedge, T3 is located on the vertical part of the wedge, and T4 is located at the outside aperture of the OBC. The OBC is analog servo controlled at 308.0 ± 0.01 K. If a temperature sensor is found to be outside the nominal limits then a flag is raised indicating that the calibration accuracy may be compromised. No such out-of-limits condition has been observed in orbit as of the date of this document.

2.1.2. Cold Space View (CSV)

There are four consecutive views of cold space centered at 75.3, 83.3, 91.6, and 100.2 degrees from nadir; referred to as S3, S4, S1, and S2 respectively. Since the scan mirror moves continuously, the effective area used for the CSVs starts at 71.8 degrees and ends at 104.5 degrees from nadir. The use of these space views during radiometric calibration is described in Section 3.1.2 of this document.

2.1.3. Onboard Spectral Reference Source (OBS)

A mirror coated with a thin film (about 10 µm thick) of Parylene was designed as the On-Board Spectral reference source (OBS) for pre-flight testing of spectrometer functionality. Figure 2-1 shows the average parylene spectra from two granules representing extremes of scan head temperature. Although the spectral features are relatively broad, they can be fitted to a precision of 1% of the FWHM of the SRF, but they are not traceable to fundamental standards. The AIRS spectral calibration (Section 4) is based on features in the upwelling spectra, which are traceable to fundamental standards.

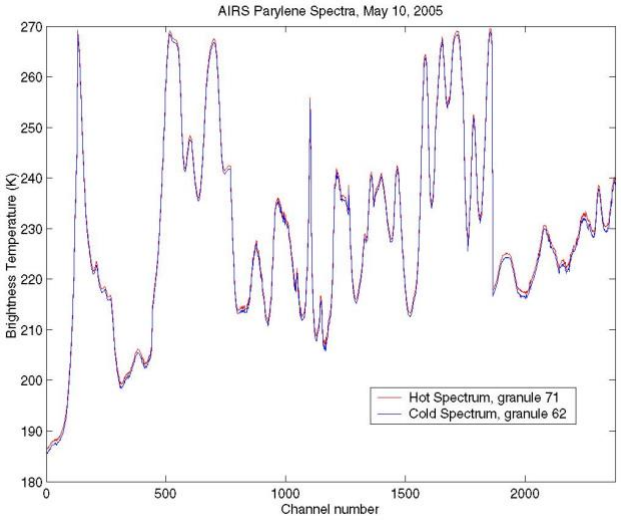

Figure 2-1: OBS spectra at cold and hot conditions

3. Radiometric Calibration

The AIRS spectrometer has 2378 spectral channels, implemented as arrays in seventeen detector modules. The first 15 modules use PV detectors and the last two use PC detectors. The AIRS Level 1B software reads the raw outputs of the 2378 channels (Level 1a) for each footprint and converts them to calibrated radiances using the AIRS radiometric calibration equation. In the following section we discuss the radiometric calibration equation (algorithm) and estimate the accuracy of the calibration.

The required absolute radiometric calibration accuracy of each AIRS spectral channel, as stated in the AIRS Functional Requirements document (Ref. 2), is the larger of (a) 3% of the radiance, or (b) 4*NEN over the full dynamic range of AIRS from 190 K to 325 K, where NEN is the Noise Equivalent Radiance. Since brightness temperature uncertainties are more intuitive than radiance uncertainty for a temperature sounder, most of the results are expressed as temperature uncertainty. The radiometric accuracy achieved in orbit has been shown to be better than 100 mK for most channels, except at extremely low scene temperatures (Ref. 7).

The Level 1B software performs the routine radiometric calibration of the AIRS data. The Level 1B output routinely generates quality assessment parameters and quality flags. These indicators are used for off-line trend analysis and are also passed on to the Level 2 (geophysical product generation) software.

The logical flow of the Level-1b process is as follows:

1) Calibration coefficient determination (offset and gain)
    a. Offset determination
        i. Determine counts-units base noise level of each channel
        ii. Determine which space observations need to be excluded from later steps:

1. South Pole contamination (Section 3.3.1)
2. Moon (section 3.3.2)
3. DC-Restore (Section 3.3.3)
4. “Pop” (Section 3.3.4)

Calculate the bias among the spaceviews for each channel, needed to adjust to an effective 90-degree viewing angle (Section 3.2)

iii. Calculate the median of the remaining bias-adjusted spaceviews in each group of 4 (Section 3.3)
iv. Calculate the offset at the start and end of each scan from a linear fit to the 10 consecutive medians

b. Gain determination
   i. Subtract the offset from the smoothed counts observing the blackbody to get blackbody signals
   ii. Determine the effective blackbody temperature as a weighted mean of the readings from the sensors plus an adjustment (Section 3.2.5)
   iii. Determine the effective blackbody radiance by applying the Planck equation to the blackbody temperature (Section 3.2.4)
   iv. Calculate the per-granule gain-adjusted nonlinearity (section 3.2.7)
   v. Calculate a gain for each scan
   vi. Final gain is granule mean of per-scan gains to reduce noise

2) Radiometric calibration by applying the calibration equation (Section 3.2.2)
3) Spectral Calibration using the calibrated radiances (Section 4)

3.1. Pre-Flight Radiometric Calibrator

Key to the precise pre-launch radiometric calibration was the large aperture blackbody (LABB) and the space view blackbody (SVBB) cold reference illustrated in Figure 3-1. Both use the same wedge cavity design. The LABB and the SVBB are traceable through their design details and the thermometry to the National Institute of Standards and Technology (NIST). The temperature sensors are model 162D Platinum Resistance Temperature (PRT) sensors manufactured by Rosemount Aerospace (now Emerson), and were provided with NIST traceable temperature calibrations accurate to ±1 mK, or better. The uncertainty of the temperature of the first surface is less than 0.05 K with all other surfaces less than 0.2 K. With more than 90% contribution from

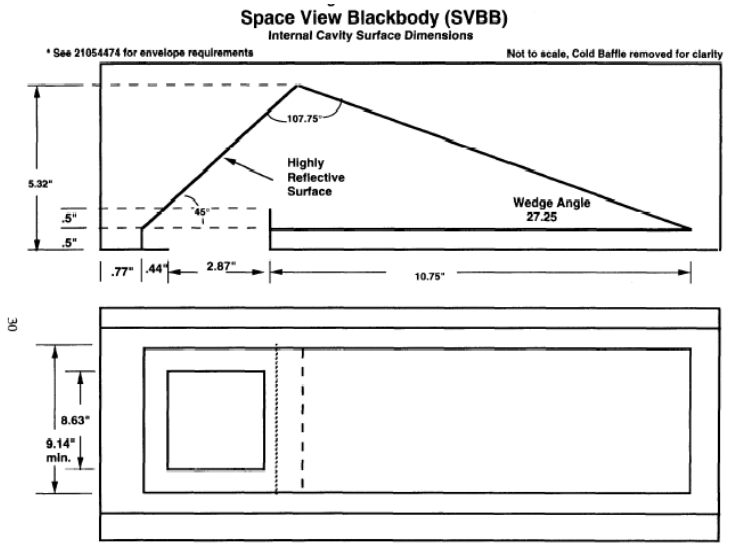

Figure 3-1: AIRS SVBB and LABB Internal Geometry

the first surface, we expect the temperature uncertainty to be better than 0.07 K.

It is coated with a specular black paint, Aeroglaze Z302, with a reflectance less than 13.5% for wavelengths below 6 μm and less than 17.5% below 15.4 μm. For the wedge angle of 27.25 degrees and the AIRS geometry, more than 6 specular reflections are required before the beam exits the cavity. The specular reflectance ($R^6 = 0.00002$) and the scattering reflectance (Ω * BRDF = 0.00004) for the two worst case conditions (both occurring at about 10 μm), results in an estimated cavity emissivity of 0.99994. The SVBB was cooled with LN_2.

In the Thermal Vacuum Chamber (TVAC), the LABB was located at a distance of 11.5 inches from the scan mirror. At this position its entrance aperture is large enough to fully contain four consecutive AIRS footprints. The LABB was transitioned from 357K to 197K and settled at each temperature plateau before acquiring data.

More details of the accuracy of the LABB is given in Ref. 7.

3.2. Radiometric Calibration Equations

The AIRS radiometric calibration involves scaling the signal sensed from the scene to that of the OBC Blackbody with a correction for the nonlinear response of the detectors and a small polarization correction. The scan mirror emission plays an important role in the radiometry due to a scan angle dependent cross polarization coupling between the scan mirror and spectrometer. With the assumption that the scan mirror emissivity is uniform, the equations reduce to a very simple analytical form with few terms, leading to reduced computational requirements for the Level 1B code and allowing for straightforward analysis of radiometric accuracy errors. Details of the pre-launch calibration are found in Ref. 8. The fundamental calibration equations have not changed significantly since launch and are found in Ref. 9 and presented below. More detail on the methodology and utilization of the pre-flight data and in-orbit data to derive the V8 radiometric and polarization calibration coefficients can be found in Ref. 10.

3.2.1. Polarization Coupling of Scan Mirror and Optics

The total signal at the detector is the sum of the radiance of the scene passed through the optics and the emission of the scan mirror also passed through the optical system. In Mueller matrix calculus, the signal is the first term of the Stokes vector, **S**, in the equation

$$\mathbf{S} = \mathbf{M_{sp}}\,\mathbf{M_{sm}}\,\mathbf{L_{ev}} + \mathbf{M_{sp}}\,\mathbf{L_{sm}} \qquad (1)$$

Where:

$\mathbf{M_{sp}}$	=	Mueller matrix for the Spectrometer
$\mathbf{M_{sm}}$	=	Mueller matrix for the Scan Mirror
$\mathbf{L_{sc}}$	=	Radiance of the Scene
$\mathbf{L_{sm}}$	=	Emission of the Scan Mirror

all evaluated at the nominal SRF centroid frequencies. In Equation 2 we give the Mueller matrix for a linear diattenuator with a fast axis θ (relative to the x-axis) and reflectance q and r in the s and p directions.

$$M = \frac{1}{2}\begin{bmatrix} q+r & (q-r)cos2\theta & (q-r)sin2\theta & 0 \\ (q-r)cos2\theta & (q+r)cos^2 2\theta + 2\sqrt{qr}\, sin^2 2\theta & \left(q+r-2\sqrt{qr}\right)sin2\theta\, cos2\theta) & 0 \\ (q-r)sin2\theta & \left(q+r-2\sqrt{qr}\right)sin2\theta\, cos2\theta & (q+r)sin^2 2\theta + 2\sqrt{qr}\, cos^2 2\theta & 0 \\ 0 & 0 & 0 & 2\sqrt{qr} \end{bmatrix} \quad (2)$$

We define θ to be the orientation and q and r to be the reflectances in the perpendicular and parallel directions, respectively, of the scan mirror. The parameters t, v, and δ are the same parameters for the spectrometer.

Assuming the scene to be unpolarized, the radiances of the scene and scan mirror are given by the vectors

$$\boldsymbol{L}_{sc} = \begin{bmatrix} L_{sc} \\ 0 \\ 0 \\ 0 \end{bmatrix} \qquad \boldsymbol{L}_{sm} = \frac{1}{2}P_{sm}\begin{bmatrix} \varepsilon_s + \varepsilon_p \\ (\varepsilon_s - \varepsilon_p)cos2\theta \\ (\varepsilon_s - \varepsilon_p)sin2\theta \\ 0 \end{bmatrix} \quad (3)$$

where P_{sm} is the Planck blackbody radiation function evaluated at the temperature of the scan mirror and ε_s and ε_p are the polarizations along the s and p direction (semi-major and semi-minor axes of the polarization ellipse), respectively.

Substituting equations 2 and 3 into equation 1 produces an expression for the Stokes vector, **S**. Since we are not analyzing polarization, we are only interested in the intensity, which is the first term of **S**

$$S_o = \frac{1}{4}P_{sm}\left[(\varepsilon_s + \varepsilon_p)(t+v) + (\varepsilon_s - \varepsilon_p)(t-v)(cos2\theta\, cos2\delta + sin2\theta\, sin2\delta)\right]$$
$$+ \frac{1}{4}L_{sc}[(q+r)(t+v) + (q-r)(t-v)(cos2\theta\, cos2\delta + sin2\theta\, sin2\delta)] \quad (4)$$

We would like to express this in terms of the mirror's average reflectance and average spectrometer transmission and polarization.

First note the identity

$$\cos\theta\cos\delta + \sin\theta\sin\delta = \cos(\theta - \delta) \quad (5)$$

and define the terms R, T, ε, p_r, p_t, and p_ε such that:

$$q + r = 2R; \quad q - r = 2Rp_r; \quad p_r = (q - r) / (q + r)$$
$$t + v = 2T; \quad t - v = 2Tp_t; \quad p_t = (t - v) / (t + v) \qquad (6)$$
$$\varepsilon_s + \varepsilon_p = 2\varepsilon; \quad \varepsilon_s - \varepsilon_p = 2\varepsilon p_\varepsilon; \quad p_\varepsilon = (\varepsilon_s - \varepsilon_p) / (\varepsilon_s + \varepsilon_p)$$

Substitution gives:

$$S_0 = L_{sc}\{RT + RTp_rp_t \cos 2(\theta - \delta)\} + P_{sm}\{\varepsilon T + \varepsilon Tp_\varepsilon p_t \cos 2(\theta - \delta)\} \qquad (7)$$

Now use:

$$\varepsilon = 1 - R$$
$$p_\varepsilon = [(1 - q) - (1 - r)] / [(1 - q) + (1 - r)] = -(q - r) / (2 - (q + r)) = -2Rp_r / 2(1 - R) \qquad (8)$$
$$p_\varepsilon = -Rp_r / \varepsilon$$

Substituting gives the expression for the intensity on the detector:

$$S_0 = L_{sc}RT\{1 + p_rp_t \cos 2(\theta - \delta)\} + P_{sm}RT\{\varepsilon / R - p_rp_t \cos 2(\theta - \delta)\} \qquad (9)$$

S_o is the total radiance as seen by the AIRS instrument at the detector from the scene and the scan mirror as modulated by the polarization.

3.2.2. Radiometric Calibration Equation

The basic approach for AIRS radiometric calibration is to perform a gain and offset (two point) correction. This first involves subtracting the space view signal from the Earth view signal for every scene and OBC position to correct for any detector and electronic zero radiance offset.

$$S_0 = S_{sc} - S_{sv} = L_{sc}RT\{1 + p_rp_t \cos 2(\theta - \delta)\} - P_{sm}RTp_rp_t [\cos 2(\theta - \delta) + \cos 2(\theta_{sv} - \delta)] \qquad (3)$$

The AIRS radiometric response is calibrated during pre-flight testing by viewing a Large Area Blackbody (LABB) at multiple temperatures simultaneously with a Space View Blackbody (SVBB). The radiances of the LABB are fit to a second order polynomial in signal counts, dn, from the AIRS instrument for every channel. Equating equation 10 to a second order polynomial in counts and solving for the scene radiance, we get the radiometric calibration equation (*RT* factor is absorbed into the polynomial coefficients).

$$L_{sc} = L_o(\theta) + \frac{c_0 + c_1(dn_{ev} - dn_{sv}) + c_2(dn_{ev} - dn_{sv})^2}{[1 + p_rp_t cos2(\theta - \delta)]} \qquad (11)$$

p_rp_t =Product of scan mirror and spectrometer polarization diattenuation (unitless)
δ = Phase of spectrometer polarization (radians)
c_0 = Instrument offset (W/m^2-sr- μm)
c_1 = Instrument gain (W/m^2-sr- μm-counts)
c_2 = Instrument nonlinearity (W/m^2-sr- μm-counts^2)

3.2.3. Radiometric Offset and Polarization

The radiometric offset, c_o, encompasses any terms on the right hand side (LHS) of Equation 11 that are independent of the scene radiance and the polarization. Preflight testing has demonstrated that the differences between the Earth view and space views are primarily due to coupling of the mirror polarization with that of the spectrometer. In Version 5 and Version 8, c_o is set to zero as it appears to be a test related artifact related to the reduced accuracy of the LABB at cold scene temperatures (Ref. 5, Ref, 7). The entire contribution of c_o is included in the uncertainties of the radiance (Ref. 7).

The polarization offset term results directly from the coupling of the scan mirror emission and the spectrometer.

$$L_o(\theta) = \frac{P_{sm}(T_{sm},\lambda)p_r p_t[cos2(\theta-\delta)-cos2(\theta_{sv}-\delta)]}{[1+p_r p_t cos2(\theta-\delta)]} \qquad (12)$$

Note that the polarization offset, L_o is obtained from polarization terms collected in-flight while viewing space (see below) completely independent of the radiometric calibration. The polarization offset is included in the calibration equation before the fit to the coefficients c_o, c_1, and c_2.

3.2.4. On-board Gain Correction

We apply a 2 point gain correction to the calibration that will correct for first order response variations from the instrument. These variations can be caused by optical or detector degradation and natural aging of the instrument. Since AIRS is a grating spectrometer, optical transmission degradation effects can be corrected using this method. By evaluating Equation 11 for the OBC view (that is, by substituting $L_{OBC} = \varepsilon_{obc}P_{obc}(T_{obc},\lambda)$ for L_{sc} and $\theta = \theta_{obc}$ =180 degrees, solving for c_1 gives the gain term. In the AIRS V8 L1B, the gain is updated once a granule to reduce noise effects.

$$c_1{}' = \frac{[\varepsilon_{obc}P_{obc}(T_{obc},\lambda)-L_o(\theta_{obc})][1+p_r p_t cos2\delta]-c_2(dn_{obc}-dn_{sv})^2-c_0}{(dn_{obc}-dn_{sv})} \qquad (13)$$

c_1' is substituted for c_1 in equation 11 for the in-flight algorithm.

Signal and Calibration target counts and engineering telemetry are required to compute the signals observed by AIRS. These include:

dn_{ev} = Digital counts while viewing Earth for each footprint and scan (counts)
dn_{sv} = Median of the digital counts of the 4 space views for each scan (counts)
dn_{obc} = Digital counts while viewing the OBC Blackbody (counts)
P_{sm} = Planck spectral radiance of the scan mirror at T_{sm} (W/m^2-sr-μm)
P_{obc} = Plank spectral radiance of the OBC blackbody at temperature T_{obc} (W/m^2-sr-μm)
T_{obc} = Temperature of the OBC blackbody (K)
T_{sm} = Temperature of scan mirror (K)
θ = Scan Angle measured from nadir in the Earth View (radians)
$\theta_{sv,i}$ = Scan Angle measured from nadir for the i^{th} space view (i=1 to 4) (radians)

Many of the other terms are derived from the instrument telemetry. The scan mirror radiance, P_{sm}, is obtained by evaluating the Planck function at the scan mirror temperature, which is determined using telemetry from a non-contact temperature sensor in a small on-rotation-axis cavity in the back of the mirror. Likewise, the OBC radiance, $\varepsilon_{OBC} \times P_{OBC}$, is calculated from the Planck function using telemetry from the four temperature sensors and the emissivity (see below). The scan angle, θ, is read out directly from the encoder on the scan motor. The data number from the earth scene, dn_{ev}, is obtained directly from the instrument analog-to-digital converter (ADC) for each channel when viewing the Earth scene. The space view counts offset, dn_{sv}, involves a slightly more complicated algorithm as discussed below. c_1 is computed for every granule (see above). The remaining terms, $p_r p_t$, δ, and c_2, are obtained from pre-flight and in-flight calibration, which is discussed is the following sections.

The evaluation of the Planck function requires the knowledge of the centroid of the SRF for each channel. A change in the SRF centroid of 5% of the SRF width would change the OBC signal by less than 19 mK. Since the SRF centroids have changed less than 5% of the SRF width, the radiometric calibration uses a fixed set of SRF centroids, referred to as the "nominal freq" in the L1B data files, as opposed SRF centroids derived by the spectral calibration for each data granule, referred to as "spectral freq". The spectral calibration of AIRS is essentially independent of the radiometric calibration. More on the spectral calibration is discussed in Section 4.

3.2.5. OBC Temperature

As described in section 2, the OBC has four temperature sensors. The measured OBC temperature, T_{OBC}, is calculated as a linear combination of these four temperatures:

$$T_{OBC} = \tau_1 T_1 + \tau_2 T_2 + \tau_3 T_3 + \tau_4 T_4 \qquad (14)$$

The four weights τ_i have been given values $\tau_1 = 0.45$, $\tau_2 = 0.45$, $\tau_3 = 0.09$, and $\tau_4 = 0.01$ based on the positions of the sensors and the recommendations of AIRS thermal engineers. By iterating the temperature offset ΔT until the effective emissivity term is near 1.0 for all channels, it was found that a value $\Delta T = 0.3$ K fits the response of AIRS to the LABB best, meaning that the temperature of the OBC as measured directly by its thermometers is low by 0.3 K. This 0.3 K correction term is reasonable when compared to the calibration offsets for the OBC blackbody temperature sensors during their calibration, the OBC blackbody thermal environment, and the electronic design of the temperature sensor readout (Ref 7).

Because the OBC is operated over an extremely narrow range of temperatures (controlled to 307.92 ± 0.05 K), the constant offset model works well in transferring the calibration of the OBC to the LABB. In a physical sense, we would like to derive the temperature offset ΔT and emissivity of the OBC blackbody. In a practical sense, we do not have enough information to solve for both. Therefore, we assume a temperature correction based on expectations from the OBC blackbody, as stated above, and consider the rest to be due to the emissivity and residual uncertainty in the temperature and other unknown terms. We call the emissivity/temperature residual term the "effective emissivity" because it is not the true emissivity of the OBC blackbody.

3.2.6. Effective Emissivity Determination

The "effective emissivity" of the OBC is the emissivity needed match the computed radiances of the LABB and OBC given the OBC temperature is fixed for all channels as defined above. Deriving the effective emissivity of the OBC in this way transfers the calibration accuracy of the LABB to the OBC and is performed for SI traceability (Ref. 7).

The OBC Effective Emissivity is obtained while viewing the LABB during the linearity testing pre-flight using equation 11 and solving for the OBC emissivity. We compute the effective emissivity directly from the linearity test with $Lo(\theta_{OBC})$ computed from equation 12 with $\theta_{OBC} = 180°$ and $cos2(180°-\delta)=cos(2\delta)$.

$$\varepsilon_{obc} = \left\{ L_o(\theta_{obc}) + \frac{c_0 + c_1(dn_{obc}-dn_{sv}) + c_2(dn_{obc}-dn_{sv})^2}{[1+p_r p_t cos2\delta]} \right\} / P_{obc} \qquad (15)$$

The effective emissivity is relatively uniform ranging from 0.998 to 1.002 across all channels, all modules and all tests, indicating the OBC blackbody matches the LABB extremely well. The variability amongst the data sets show only slight A/B dependence which is carried in the V8 calibration. Finally, the emissivity for all channels is fit to a 3rd order polynomial with wavelength to reduce test related discontinuities at module boundaries. Deviations from this fit are included in the radiometric uncertainty.

3.2.7. Nonlinearity

During T/V testing, the AIRS viewed the LABB and the SVBB with the instrument scanning in the normal mode. The radiometric response was measured by stepping the LABB over multiple temperatures: 205 K, 220 K, 230 K, 240 K, 250 K, 265 K, 280 K, 295 K, and 310 K. The LABB was temperature stabilized at each level and more than 100 scans of AIRS data acquired. The digital counts, dn, from the AIRS corresponding to the peak footprint and ±2 footprints and all scans were averaged and used in equation 11 with the calculated LABB radiances to solve for the radiometric calibration coefficients, $c_0, c_1,$ and c_2. The coefficients are computed from several tests performed pre-flight at different times for the A side, B side and AB side detectors (Ref. 10). Consistency was seen amongst the detectors in the modules and between tests with the normalized nonlinearity coefficient.

$$c_2' \equiv \frac{c_2}{{c_1}^2} \qquad (16)$$

The normalized nonlinearity coefficients are averaged over all test to produce a single set for all times. The regular nonlinearity term, c_2, is updated every granule with the approximate granule gain. Here the gain is not corrected for polarization and nonlinearity (as done in equation 13) since the gain is only used to adjust the nonlinearity and their contribution is negligible.

$$c_2 = c_2' \times \left(\frac{L_{OBC}}{(dn_{OBC}-dn_{sv})} \right)^2 \qquad (17)$$

3.2.8. Polarization Amplitude and Phase

Version 8 of the Level 1B uses an empiricalmethod for determining the polarization amplitude and phase for the scan mirror, $p_r p_t$ and δ compared to prior versions. The AIRS views space at four different mirror positions every scan. We can use this feature to extract the polarization response terms from the signals observed in the space views. Figure 3-2 shows the orientation of the scan and location of the space view and on-board calibrators.

Starting with equation 11, and setting $L_{ev} = 0$, and substituting equation 12 we get

$$0 = \frac{P_{sm} p_r p_t [cos2(\theta-\delta)+cos2\delta)] + a_1'(dn_{ev}-dn_{sv}) + a_2(dn_{ev}-dn_{sv})^2}{[1+p_r p_t cos2(\theta-\delta)]} \quad (18)$$

Ignoring second order terms (the polarization signal is small so a nonlinear correction to the polarization is negligible)

$$(dn_{ev} - dn_{sv,i})\, c_1' = -L_{sm} p_r p_t \left[cos2(\theta_{ev} - \delta) - cos2(\theta_{sv,i} - \delta)\right] \quad (19)$$

This relationship is true for all positions of the mirror, not just the earth view. Applying the equation for each of the space views relative to space view 1 and using the trig relationship,

$$cos2(\theta - \delta) = cos2\theta cos2\delta + sin2\theta sin2\delta \quad (20)$$

we can write the signal observed in the space view i = 2, 3, or 4 relative to space view 1.

$$\left(dn_{sv,i} - dn_{sv,1}\right)c_1' = -L_{sm} p_r p_t \left[cos2\theta_{sv,i} cos2\delta + sin2\theta_{sv,i} sin2\delta + cos2\delta\right] \quad (21)$$

or

$$\frac{-\left(dn_{sv,i}-dn_{sv,1}\right)c_1'}{L_{sm}} = d_1\left(1 + cos2\theta_{sv,i}\right) + d_2 sin2\theta_{sv,i} \quad (22)$$

where

$$d_1 = p_r p_t cos2\delta \quad (23)$$

$$d_2 = p_r p_t sin2\delta \quad (24)$$

We can fit the above equation using linear regression and solve for the coefficients

$$p_r p_t = \sqrt{d_1^2 + d_2^2} \quad (25)$$

For this version, $p_r p_t$ is always positive. The phase is calculated using equations 23 and 24 as

$$\delta = \frac{1}{2} tan^{-1}\left(\frac{d_2}{d_1}\right) + \delta_o \quad (26)$$

where the phase offset, δ_o, depends on the quadrant of the argument of the inverse tan function and the offset computed for other channels in the module Specifically,

$$\delta_o = \begin{cases} 0 & for \quad d_1 > 0 \\ -\frac{\pi}{2} & for \ d_1 < 0, d_2 < 0 \\ \frac{\pi}{2} & for \ d_1 < 0, d_2 > 0 \end{cases} \quad (27)$$

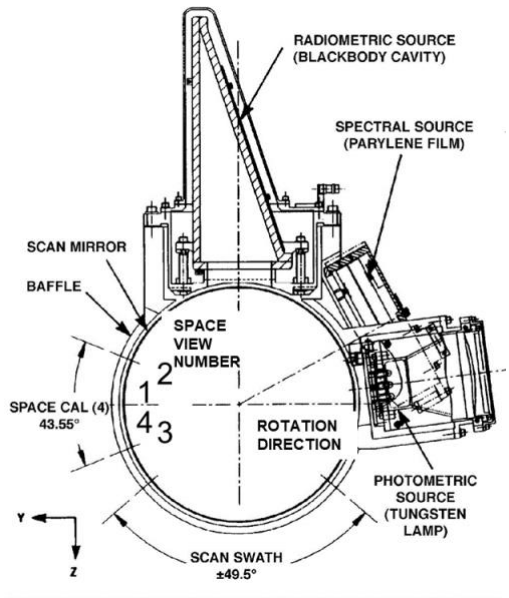

Figure 3-2: Relative position of Scene View, Space Views and Blackbody.

with $\delta_o = \delta_o \pm \pi$ applied to channels as needed to reduce variability of phase amongst all channels in the module.

The average counts for each of the 4 space views, $dn_{sv,i}$, for each day of the AIRS mission was collected and then averaged into values for each month. Data are filtered for bad space view 3 during certain parts of the orbit and averaged into 224 months from January 2003 through January 2022. The 4 space views for each month are used to compute the polarization product, $p_r p_t$, and phase, δ, from equations 23-27 for each channel and month. The data are sorted into A side, B side and AB side channels and the results interpolated for all channels so that we end up with a polarization for each channel and A, B and AB sides. For each channel and AB side, a linear fit over all months is computed for each $p_r p_t$ and δ, and an offset and trend calculated. The end result is time dependent and AB side dependent polarization coefficients for all channels shown in Figure 3-3.

A 10 point running smooth amongst channels is applied to all coefficients within each of the 17 modules for each A, B and AB side. The smooth uses the median of the 10 point window which is centered on the channel. The size of the window reduces accordingly at the edges of the modules. The smooth is necessary to reduce channel-to-channel noise inherent in the coefficients due to the instrumental noise present during the calibration. Since the variation of coefficients amongst the channels is usually slowly varying within a module, the smoothing has little impact on the radiometry, other than reducing the noise.

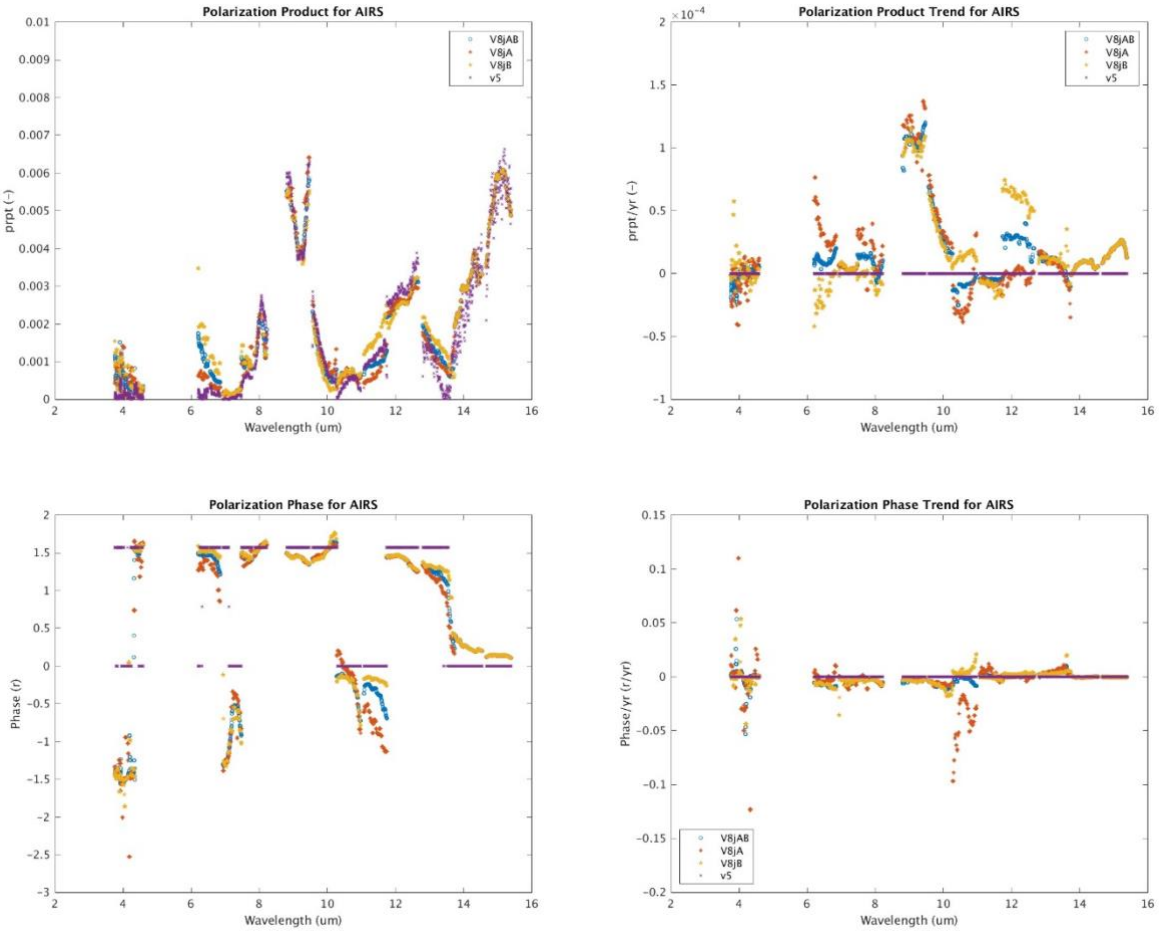

Figure 3-3 Top Left) Polarization amplitude for 2003 for V8 compared to V5. Top Right) Polarization amplitude trend. Bottom Left). Polarization phase for 2003 for V8 compared to V5. Bottom Right) Polarization phase trend. V8 polarization is derived from in-flight space views.

3.2.9. Relative Contribution of Individual Terms in the Radiometric Calibration

We can examine the contribution of the offset, gain and nonlinear terms in the calibration equation. This allows us to understand what instrumental behaviors are driving the radiances in any given part of the spectrum. We can rearrange the equation 11, 12, and 13 to provide 4 primary terms

$$L_{ev} = L_{\mathrm{op}}(\theta) + L_{\mathrm{of}}(\theta) + L_1(\theta) + L_2(\theta) \tag{28}$$

The first term represents the offset due to polarization:

$$L_{\mathrm{op}}(\theta) = L_{\mathrm{o}}(\theta) - L_o(\theta_{obc}) \frac{(dn_{ev} - dn_{sv})}{(dn_{obc} - dn_{sv})} \frac{[1 + p_r p_t cos2\delta]}{[1 + p_r p_t cos2(\theta - \delta)]} \tag{29}$$

The second term represents the offset in the fit to the LABB (set to zero in V5 and V8)

$$L_{\text{of}}(\theta) = \frac{c_0\left[1-\frac{(dn_{ev}-dn_{sv})}{(dn_{obc}-dn_{sv})}\right]}{[1+p_r p_t cos2(\theta-\delta)]} \quad (30)$$

The third term represents the first order response (gain)

$$L_1(\theta) = [\varepsilon_{obc} P_{obc}(T_{obc}, \lambda)] \frac{(dn_{ev}-dn_{sv})}{(dn_{obc}-dn_{sv})} \frac{[1+p_r p_t cos2\delta]}{[1+p_r p_t cos2(\theta-\delta)]} \quad (31)$$

The fourth term represents the contribution of the nonlinearity.

$$L_2(\theta) = \frac{c_2}{[1+p_r p_t cos2(\theta-\delta)]}[(dn_{ev}-dn_{sv})^2 - (dn_{ev}-dn_{sv})(dn_{obc}-dn_{sv})] \quad (32)$$

Figure 3-4 shows the contribution of the four contributors to the AIRS radiances for a scene temperature of 250K at nadir for the AB sides. We separated out the contribution of the polarization static dependence and the trend due to the polarization.

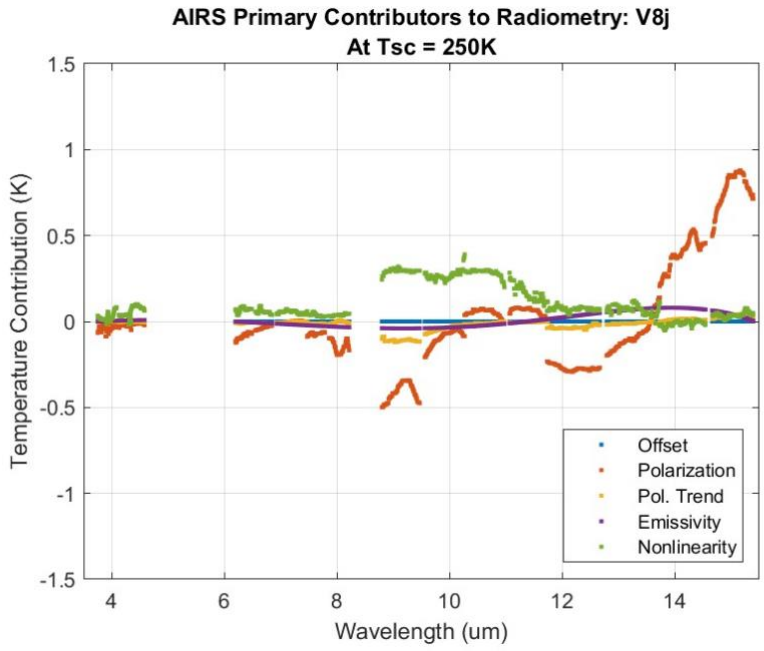

Figure 3-4: Key contributors to the AIRS radiances at 250K for AB side channels including Mirror Polarization, 'Effective' Emissivity and Nonlinearity.

3.2.10. The A, B and A+B Effect

In order to achieve a high degree of reliability, the AIRS instrument makes use of system and subsystem redundancies. This includes a focal plane, where the each of the detectors (except for the M11 and M12 detector modules), has an A and B side, and an associated A and B side electronics readout and ADC. The on-board data formatting system then combines the signal using an up-loadable Channel Weight table. The weight can be set to 0 (A+B), 1 (A only) or 2 (B only). For most channels the weight has been zero since launch. A failure in a detector or its associated electronic chain (e.g. due to a strong radiation

hit) can thus be corrected by adjusting the A/B weights. In the previous releases of the L1B calibration (Version 5 and earlier) the calibration coefficients did not distinguish between A/B states. However, a change in the A/B state creates discernable effects at the 100 mK level at extremely low scene temperatures. The V8 release uses A and B state dependent radiometric coefficients (Ref. 10). The change not only uses the coefficient relevant to the A/B side for a given time in history of the AIRS, but also allows a change to occur in the future without adversely impacting the calibration accuracy.

3.3. Space-View Processing

Every signal measured by AIRS is the combination of the signals from the target radiance, the thermal emission of the AIRS instrument, and the electronics offset. The signal, in data numbers, associated with thermal emission and electronics offset, $dn_{sv,I}$, varies with time and is deduced from views of cold space. Associated with each cross-track scan are four space view measurements called S3, S4, S1 and S2. The space views occur while the AIRS boresight vector is at 75.3, 83.3, 91.6 and 100.2 degrees from nadir, respectively, while the Earth horizon is at 61 degrees from nadir. Space view S2 is followed by a view of the blackbody at a 180-degree scan angle. The cycle repeats every 2.667 seconds. Figure 3-2 illustrates the logical progression of the cross-track scan. Note the relative ordering of the space views. The views are generally treated as a single group, however, as explained in Section 3.3.4, discontinuities may occur between the S4 and S1 views. In that case, we may consider the space views acquired in the order S1 - S4 as a logical unit.

Prelaunch there was a concern that contributions from the Earth's limb might contaminate the space views, possibly requiring that S3 be excluded from offset calculations. Figure 3-5 shows the actual observed biases of the four space views as a function of AIRS channel number. While real biases are observed, their magnitudes are less than 0.1 K for a 250 K scene. Furthermore, the four space views do not show a monotonic change as one moves away from the Earth's limb, contradicting the pre-flight expectation. In fact, the radiometric differences in the four space views follows the expected emission due to polarization. This was confirmed during the Deep Space Maneuver (DSM) on 9/23/2021. For all scans, all four space views are used to calculate the offset signal. In Version 8, a granule-wide median offset between S1 and the other 3 spaceviews is calculated first, and then this offset is subtracted from each spaceview before the next stage. These offsets are a

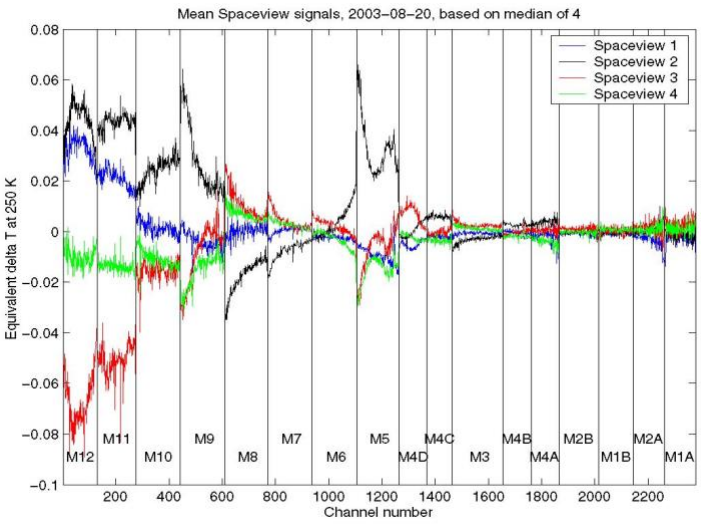

Figure 3-5: The difference between the four spaceviews can be measured, but they are less than 0.1 K equivalent for a 250 K scene.

direct measurement of the polarized emission. Removing them from the space view calculation reduces noise and should reduce biases in cold scenes. S1 is used because it is closest to 90 degrees from nadir.

In order to reduce or eliminate possible outlier effects (especially spikes caused by radiation events), the $dn_{sv,i}$ are calculated from medians of consecutive space views. That is, for each group of adjacent space views S3, S4, S1, and S2, a median value of the signal is calculated. The standard definition of a median is used: for four space views, we take the average of the 2nd and 3rd ranked values. In cases where some space views are filtered due to south-pole contamination, discontinuities, or moon contamination, the median may be just the value of the one remaining space view or the average of two remaining space views. To further reduce the radiance error due to drifts in the offset, the $dn_{sv,i}$ are calculated by performing a linear fit (in time) to the five space view medians before the scan of interest and the five space view medians after the scan of interest. This method, calculating medians of groups of four space views and fitting linearly in time to ten such medians, forms the basis of the AIRS IR offset calculation, but several factors discussed in the following complicate the implementation.

In order to support the analysis of potential degradation of the calibration due to scan mirror contamination, the mean, max and min space view signal determined from each detector for each data granule are saved.

There are indications when viewing 225 K and colder scenes, that at the 100 mK level there is an A/B dependent effect in the M7 and M8 detector modules, which was not accounted for in the V5 calibration. This effect may be related the zero-point determination using the SV. The V8 changes do not correct for this effect, but the resulting error is included in the V8 radiometric uncertainty.

3.3.1. South Pole spaceview contamination

After launch, it was observed that contamination increased the signal seen in the spaceviews closest to Earth in the shortwave spectral region when the spacecraft was near the South pole. The cause of this stray signal is under investigation. Spectrally, the modules most affected are M2b and M2a, as shown in Figure 3-6. Spatially, the effect is localized near the south pole but moves with the seasons, as shown in Figure 3-7.

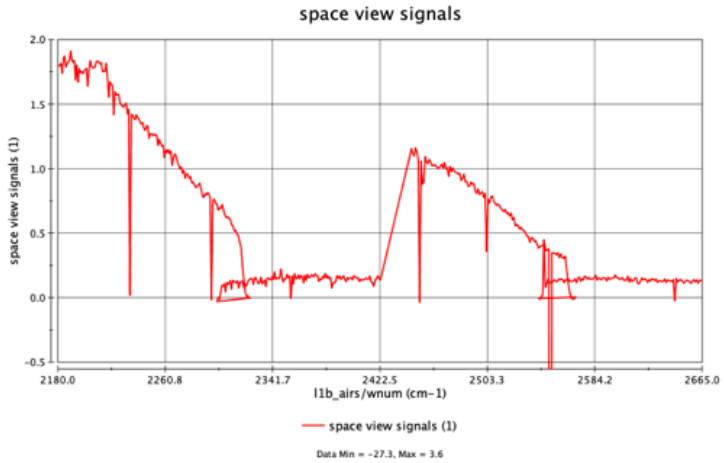

Figure 3-6. Excess signal (counts) for descending 80-90 degrees September 2019 (counts).

Spaceview 1	Spaceview 2	Spaceview 3 (closest to Earth)	Spaceview 4 (second closest to Earth)
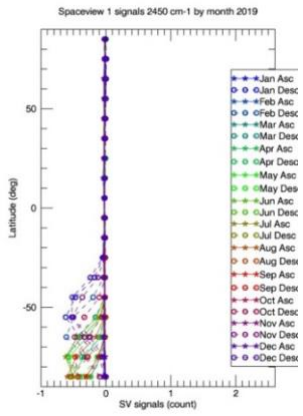	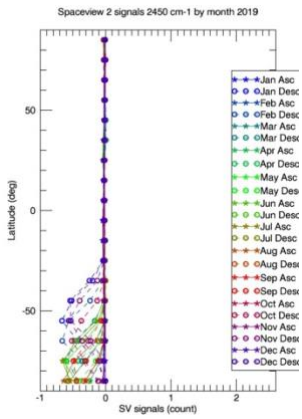	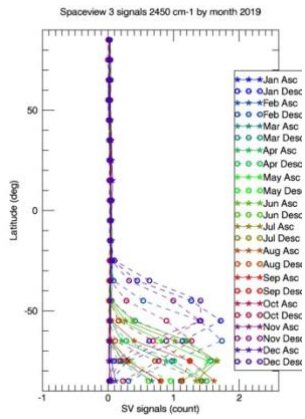	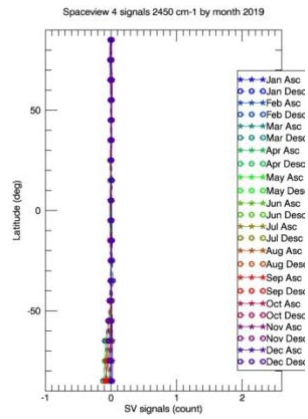

Figure 3-7. Spaceview signals for the 2450 cm^{-1} channel by month for 2019 as a function of longitude for the four spaceviews.

To prevent the spaceview contamination from affecting calibration, space view 3 is excluded from use in calibration of modules m2a and m2b for the ranges listed in Table 3-1, which correspond to where the contamination is greater than 0.1 count. Space view 4 is also excluded for a smaller range, starting 10 degrees later and ending 10 degrees sooner.

Table 3-1. Boundary latitudes for significant impacts on spaceview 3.

Month	Descending North latitude boundary	Descending South latitude boundary	Ascending South latitude boundary	Ascending North latitude boundary	Total latitude range (degrees)
Jan	30	80			50
Feb	40	90		80	60
Mar	50	90		70	60
Apr	60	90		60	60
May	70	90		50	60
Jun	70	90		50	60
Jul	70	90		50	60
Aug	60	90		60	60
Sep	50	90		70	60
Oct	40	90			50
Nov	30	80			50
Dec	20	60			40

3.3.2. Moon-in-View

The moon is visible in AIRS space views at accurately predictable times. This occurs roughly six months per year, for two to three days of those months, for one or two granules in each orbit of those days. When this happens, the moon is usually present in only one of the four space views and the median algorithm successfully excludes it as an outlier. It can also happen that the moon is present in two consecutive space views, which would badly skew the median. Consequently, an algorithm has been implemented to identify space views containing Moon contamination and excludes them from the median calculations.

A simple 15-channel test used in version 4 was found to miss some Moon events, so starting with version 5, and continued in version 8, it was replaced with a more robust "short wavelength, long-wavelength plus Moon geometry" algorithm:

1. Moon detection is performed, independently, by the 514 short-wavelength channels in Modules 1A, 1B, 2A, and 2B and the 662 long-wavelength channels in Modules M7, M8, M9, and M10. Channels with an AB State > 2 are excluded.
2. Continue looking for brightness changes with a sliding window of 8 space views (Figure 3-8) that incorporates the last two footprints (SV 1 and 2) of the previous scan, four from the current scan (SV 3 and 4 before, then SV 1 and 2 after, the Earth scenes) and the first two footprints of the following scan (SV 3 and 4 again).
3. Continue calculating relative changes in detector counts within each 8-SV window (for each channel), based on the smallest count value within that window. Convert each set of eight delta-counts into Noise units by a fixed reference value for each channel. In this new algorithm, however, all the Noise values of the 500+ channels in each Moon channel set are collected, the top and bottom 10% discarded, and a single mean calculated for each 8-SV data set. This produces – for each scan line – two independent data sets: 8 mean Noise levels for the short- and 8 mean Noise levels for the long-wavelength sets.
4. The Moon in View (MIV) Noise threshold varies with Moon separation angle for each space view footprint. Note that although this angle is updated every scan, the angle for SV 'n' of the current scan can also be used for SV 'n' of the adjacent scan, within that same window. This helps us at the start and end of a granule when the 8-SV window extends past a granule boundary (i.e., before Scan 1 and after Scan 135).
5. Now divide the Moon separation angle into along-track and cross-track components to create a "box" into which Moon may be located. For Moon separation angles of 30 degrees or more, the along-track component is negligible. Therefore, using the larger dimension of the box as a criterion, apply the following Noise thresholds that were developed over several MIV examples:

    a. For angles less than 0.25 degrees, threshold = 1.4 Noise units
    b. For angles less than 0.50 degrees, threshold = 1.7 Noise units
    c. For angles less than 0.70 degrees, threshold = 2.1 Noise units
    d. For angles less than 0.85 degrees, threshold = 3.0 Noise units
    e. For angles less than 1.30 degrees, threshold = 3.5 Noise units
    f. For angles beyond 1.30 degrees, threshold = 4.0 Noise units
    g. For angles that are missing / invalid data use 3.5 Noise units

6. Note that each of these 16 mean Noise data values for the current scan are independent and any one can set the MIV flag for the current scan to TRUE. However, this PGE also retains a [8 footprint x 135 scan] matrix to maintain a record of exactly which footprints were flagged to omit them from subsequent NeN and offset calculations.

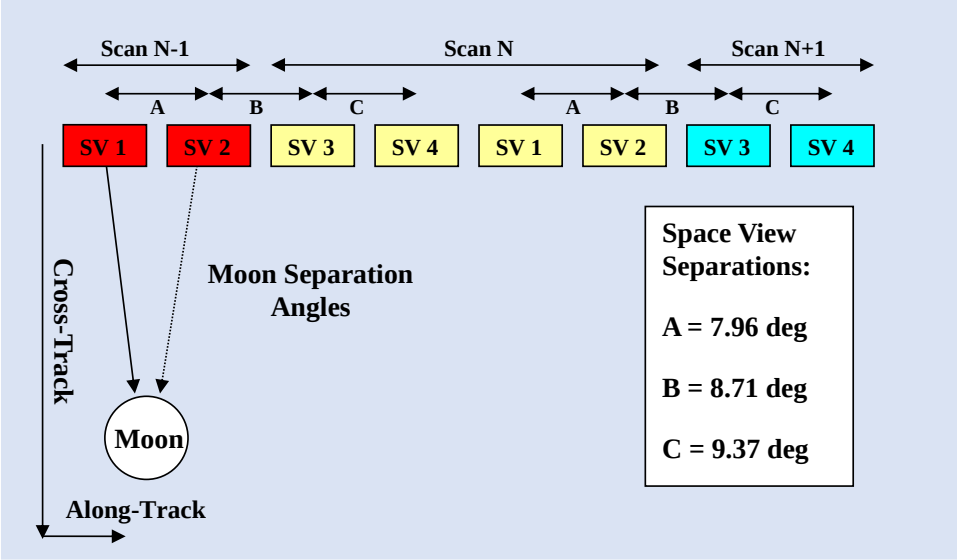

Figure 3-8 Illustration of the Moon avoidance algorithm. While the data is flagged as potentially Moon contaminated, the moon-in-view algorithm appears to handle this situation sufficiently well that no radiometric effect has been detectable in the V5 data. There is no change in the V8 PGE.

3.3.3. DC Restore

The analog output voltage of all 2378 AIRS channels is sampled simultaneously using a per-channel sample-and-hold capacitor. The conversion from analog to digital is done sequentially. A large fraction of the signal from PV modules M3-M10 is due to instrument background, i.e. the infrared radiation from the spectrometer, and electrical offset due to dark currents. To digitize the signal more accurately (and quickly), the analog signal is read as the difference between the sample-and-hold capacitor and a DC restore capacitor of each channel. The DC restore capacitor discharges with a slow exponential decay, with time constants varying from an estimated mean of 90 minutes in M8 to over 1000 minutes in M5. Because of the way the readout electronics are connected, this results in the digitized signal decreasing with time (for all measurements) in modules M3-M5 and increasing with time for modules M6-M10. For this reason, the DC restore capacitors are periodically refreshed in an event referred to as the DC Restore (DCR). The DCR time is on-orbit commandable and was set to 20 minutes during pre-launch testing and has remained at that value so far in the mission. The DCR occurs between scans (the end of the dwell period associated with viewing S4, but before S1) and results in a discontinuity in signal level between S4 and S1. The times of these DCRs are identified in downlink telemetry. It was discovered during instrument testing that the first space view following a DCR (S1) is always invalid for DC restored channels. For this reason, it is excluded from the median calculations. There is no change in the V8 release.

3.3.4. Fitting Across Space View Signal Discontinuities

The linear fit in time to the ten space view count medians is straightforward when the data varies smoothly, but when a step occurs in the data (due to a data dropout, a DCR, or a pop), additional steps are required in the Level 1B algorithm. The process is illustrated in Figure 3-9. When a DCR is indicated in telemetry, it is known to have occurred after S4 and before the following S1. All channels in modules M3-M10 experience a discontinuity in their signal levels at this time, precluding a simple fit. For each of these channels, two one-sided fits are performed first. The median of the two space views immediately prior to the discontinuity (S3 and S4, filtered for possible moon contamination) is calculated, as are medians for the nine preceding groups of four space views. In the event that a pop is detected for a channel sometime during the nine scans before the DCR, then only medians after the pop are used. A straight line is fit to these median values in time and an offset, dn_{pre}, is calculated corresponding to the time of the discontinuity. For a detailed description on what is considered a "pop" or "popping", see the relevant entry in the FAQ.

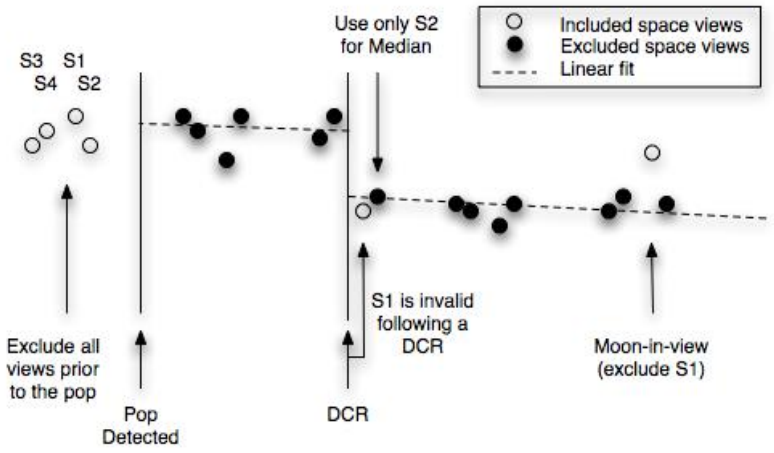

Figure 3-9: In L1B, space views only after a pop or DCR are used in the offset fit.

Likewise, a fit is performed to the space views following the DCR discontinuity. The median of the two space views immediately after the discontinuity (S1 and S2, filtered for possible moon contamination) is calculated, as are medians for the nine following groups of four space views. In this case, the S1 view immediately following the DCR is invalid, so the median of the two space views is simply the value of S2. In the event that a pop is detected for this channel sometime during the nine scans after the DCR, only medians before the pop are used. A straight line is fit to these median values (ten nominally, absent any pops) in time and an offset, dn_{post}, is calculated corresponding to the time of the discontinuity.

The difference dn_{pre} - dn_{post} is added to space views following the discontinuity and a fit to the ten (now smoothed) medians is calculated as described above. Finally, the difference, dn_{pre} - dn_{post}, is subtracted from the fit values following the discontinuity. Discontinuities introduced by pops are handled similarly (difference added in, fit to, and subtracted back off), but with two differences: First, pops detected by the Quality Assurance (QA) algorithm occur during the scene portion of a scan between space views S2 and S3 instead of between space views S4 and S1. Second, the magnitude of the discontinuity correction comes from the pop detection QA rather than from the two one-sided linear fits used with DCRs. The scan line during which a pop occurs is identified in the Level 1B output.

3.4. Radiometric differences between V5 and V8

The radiometric differences between Version 5 of the Level 1B PGE and Version 8 are deterministic, aside from small differences associated with the space view handling. Figure 3-10 shows the computed difference for the nadir viewing position and scene temperatures ranging from 220K to 300K. The changes are mostly less than 200mK with the biggest changes occurring at colder scene temperatures due to changes of the polarization terms. More information on the differences between V5 and V8, see the AIRS L1B Version 8 Test Report.

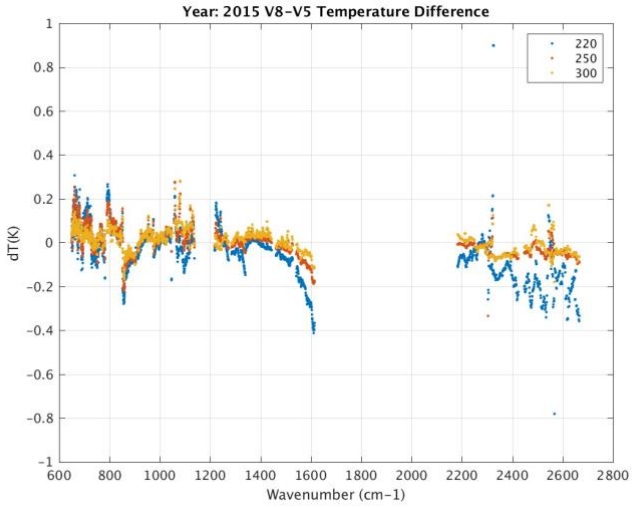

Figure 3-10. Theoretical scene temperature difference between Version 5 and Version 8 for nadir vs scene temperature.

3.5. Noise and Uncertainty

3.5.1. Instrumental Random Noise

The random noise was characterized pre-launch and during special on-orbit tests. Digital instrument output from calibration targets held at a known temperature was acquired pre-launch and used to characterize the noise. In this test, the AIRS scan mirror was locked at the calibration target for 20 minutes while data are collected. For AIRS, data were acquired while viewing the Space View Blackbody (SVBB), and the Large Area Blackbody (LABB). Radiometric sensitivity is expressed as the Noise Equivalent Radiance (NEN) for a scene temperature of 250 K: NEN250. On-orbit the NEN is measured for every granule by analyzing the standard deviation of the OBC and SVS measurements for each of the 135 scan lines in one granule for each detector. Figure 3-11 shows the NEN calculated for a single granule in 2015 (Ref. 5). The NEN250 for AIRS is measured by interpolating the noise while viewing cold space and the OBC at 308 K according to Equation 33.

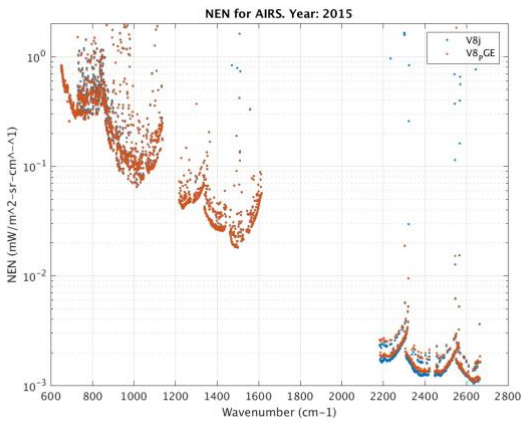

Figure 3-11. Noise Equivalent Radiance for AIRS from the V8 PGE and the V8 Testbed.

$$NEN250 = Gain \times \sqrt{\frac{L_{sc}}{L_{OBC}}\left(\sigma^2_{dn\_OBC} - \sigma^2_{dn\_SV}\right) + \sigma^2_{dn\_SV}} \qquad (33)$$

Where

Gain = Radiometric Gain (W/m^2-sr-μm / counts)

σ_{dn_OBC} = standard deviation of signals (counts with offset subtracted) when viewing OBC

σ_{dn_SV} = standard deviation of signals (counts with offset subtracted) when viewing the four spaceviews

$\frac{L_{sc}}{L_{OBC}}$= the ratio of radiance at 250 K to the radiance at the OBC temperature

3.5.2. Radiometric Measurement Uncertainty

A detailed radiometric uncertainty model was developed for the AIRS Version 5 Level 1B product (Ref. 7). In general, the AIRS radiances are accurate to better than 200mK, 1-sigma, for most channels and at scene temperatures warmer than 250K. The predictions for Version 8 are expected to be similar to those presented in the reference for Version 5, but slightly better due to the improved characterization of the instrument polarization. Shorter wavelength modules (M1-M2) have higher uncertainties at lower scene temperatures when expressed in temperature units due to the wavelength and temperature dependence of the Planck function. M8 has an A vs B bias with scene temperature that is not corrected in either version and contributes to the higher uncertainty in that module.

The AIRS instrument was designed to produce accurate absolute radiances of "climate quality". The essential accuracy of the first-principles-based estimate of the absolute accuracy has by now been confirmed. The 0.2 K (1-sigma) absolute accuracy has been validated using comparisons with the NOAA NESDIS generated Real-Time Global Sea Surface Temperature (RTGSST) and the Canadian Meteorological Centre Sea Surface Temperature (CMCSST) for scene temperatures between 285 K and 305 K (Ref. 11). Absolute accuracy at the 100 mK level has been verified using five underflights with the SHIS (Ref.12.) and observation from Concordia Station at Dome C (Ref. 13). Analysis using the first seventeen years of AIRS RTGSST observations indicates that any trend in the absolute calibration is less than 10 mK/year (Ref. 14). A more recent analysis (Ref. 15) indicates that many AIRS channels are stable to better than 3 mK/year.

4. Spectral Calibration

The AIRS spectrometer has a spectral resolution, $R = \nu/\Delta\nu$, nominally equal to 1200, where ν is the Spectral Response Function (SRF) centroid frequency in wavenumber units, and $\Delta\nu$ is the SRF full width at half its maximum response (FWHM). The AIRS Radiative Transfer Algorithm (AIRS-RTA) needs extremely accurate SRFs for each AIRS channel to ensure that uncertainty in the calculated radiances due to SRF uncertainties are much less than the AIRS radiometric calibration biases. The absolute position of the spectral response centroid and the shape of the spectral response (normalized to unity) characterize the SRF of each channel. Based on the effect of SRF shape and position uncertainty on the accuracy of the upwelling spectrum calculated by the forward algorithm, the AIRS Functional Requirements Document (FRD) (Ref. 2) called for a knowledge of channel centroid frequencies, ν, to within 1% of $\Delta\nu$ at all times. The FRD also stipulates that the SRF centroids are not to vary by more than 5% of $\Delta\nu$ over any 24-hour period. This requirement led to the inclusion of an active temperature control of the spectrometer. As a result, the SRF centroids have not changed by more than 1% of the SRF width since 2002.

The shape of these SRF's using a Bruker Instruments Model IFS-66V laboratory grade FTS interferometer was a pre-launch calibration task and therefore is not part of the Level 1B algorithms. Details of the pre-launch calibration are given in Ref. 16 and Ref. 17.

The AIRS spectral calibration is to first order a function of the temperature of the grating (which can be set by ground-command) and the temperature of the focal plane detector assembly (which can be set by ground-command). To second order the spectral calibration is also a function of the instrument's thermal environment, which is related to the solar beta angle and the length of the eclipses (which varies seasonally), to the solar zenith angle (a day/night side of the orbit and orbit position, i.e. latitude) and the length of the eclipses. The thermal environment is also influenced by the temperature of the heat exchanger on the Aqua spacecraft and the operating status of neighboring instruments on the platform, mainly AMSRE and MODIS. The radiative exchange between the surface and the AIRS instrument, which is readily seen in an orbital change in the scan mirror temperature, may also influence the spectrometer temperature. The “at launch” Level 1B PGE V5 includes a spectral calibration once per data granule (6 minutes of data) (Ref. 17).

4.1. Conceptual Approach

The AIRS in-orbit infrared spectral calibration uses identified features at known spectral locations in observed upwelling radiance spectra. It is based primarily on two components: 1) A focal plane detector assembly model and 2) A spectrometer grating model.

The focal plane detector assembly models specify the position of each AIRS infrared detector on the focal plane assembly, relative to the other detectors. A different focal plane detector assembly model is used for each of three spectrometer thermostat set-points (149 K, 155 K, and 161 K) used during pre-launch calibration. Three precision screws in the Actuated Mirror Assembly (AMA) can be turned in flight, finely repositioning the focusing mirror. The AMA was critical pre-launch for the optimization of alignment of the exit slit on the detector array. The AMA has not been used on-orbit.

The spectrometer grating model specifies the relation between detector SRF centroids and detector physical positions (relative to the grating and the imaging optics). The "at launch" L1B V5 spectral calibration (17) assumed that, for a given instrument condition (spectrometer temperature and optics alignment), the focal plane detector assembly, the relative positions of the entrance slits and relative positions of the dispersed images of the entrance slits on the focal plane remain invariant. The observed spectrally resolved features in the upwelling radiances provide "tie-points," allowing the absolute position of the focal plane detector assembly to be determined.

The validity of the spectrometer grating model has been borne out by three types of tests performed pre-launch:

A) Detector response centroids were measured before and after acoustic and vibration testing. Differences observed in detector SRF centroid (corresponding to 13% of $\Delta\nu$) were consistent with a shift of the focal plane assembly relative to the spectrometer optics.
B) Detector response centroids were measured in both +1g and –1g environments (to estimate the magnitude of zero-g release effects). Differences observed in detector SRF centroids (corresponding to 3% of $\Delta\nu$) were consistent with a shift of the focal plane assembly relative to the spectrometer optics.
C) Detector response centroids were measured repeatedly during an extended (24-hour) test simulating 14 day-night heating cycles. Again, differences observed in detector SRF centroids (this time corresponding to just 0.25% of $\Delta\nu$) were consistent with a shift of the focal plane assembly relative to the spectrometer optics.

4.2. Spectrometer Model

Although the AIRS spectral calibration ultimately reports the spectral calibration of all channels in wavenumber units, the calibration equations are in wavelength units, which are the natural units for a grating spectrometer. In principle, the positions of the SRF centroids are given by the standard grating equation,

$$m\lambda_i = d\left(\sin\alpha_i + \sin\beta_i\right), \tag{34}$$

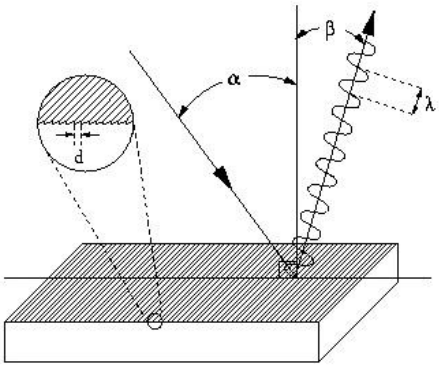

Figure 4-1: Sketch showing the basic elements of a grating spectrometer. α is the angle of incidence; β is the angle of refraction; and d is the groove spacing.

where m is the grating order, λ_i the wavelength of the i^{th} channel, d = 77.560 mm is the groove spacing of the grating, α_i is the angle of incidence and β_i is the angle of diffraction (See Figure 4-1). Because of the layout of the AIRS entrance slits, the incidence angle α_i takes on one of two values, 0.55278 or 0.56423 radians, depending on which detector array is being considered.

The actual AIRS spectrometer is folded with a considerably more complicated layout, but the basic Equation 34 applies. AIRS is a grating array spectrometer with 2378 channels. These channels are

grouped in 17 short arrays, also referred to as detector modules. AIRS works in grating orders 3 (at the longest wavelengths) to 11 (at the shortest wavelengths). Through the use of two spectral bandpass filters for each detector, one covering the spectrometer entrance slit, the other directly over each detector array, and geometric optics, each detector array is guaranteed to observe radiation from only one grating order.

From the geometry of the AIRS optics, the diffraction angle β^k_i corresponding to the center of the i^{th} detector in the k^{th} array is given by

$$\beta_i^k = \arctan \frac{y_i^k}{F_k + \Delta F} \tag{35}$$

F_k is the effective distance from the focusing mirror to the k^{th} detector array (very nearly equal to the focal length of the focusing mirror and ranging from 226313.30 to 227178.05 μm), y_i^k is the distance (in the dispersed direction) from the optical axis to the center of the i^{th} detector in the k^{th} array and ΔF is the along-focus displacement. ΔF=0 for the pre-launch calibration. The very precise 50 μm spacing of AIRS detectors within an array then allows us to write

$$y_i^k = y_0^k + (50\mu m)i + \Delta y_0 \tag{36}$$

Equation 36 is the focal plane model. In principle, this leaves us (for each "instrument temperature condition") just two parameters (per detector module), y_0^k and F_k, to determine the wavelength λ_i of each channel using Equation 34. Δy_0 is the along-dispersed displacement and is set to zero for the pre-launch calibration.

4.3. SRF Centroid Determination in Orbit

The determination of the model parameters y_0^k, Δy_0, ΔF and F_k in-orbit is the task of the spectral calibration of the L1B PGE. This is accomplished by comparing the positions of spectral features in the upwelling radiance against pre-calculated upwelling radiance features at known frequencies. Because radiative transfer in thermodynamically stable atmospheres is readily computable, and because absorption/emission line positions and strengths are well measured, the frequencies of the selected spectral features are also extremely well known. The rate at which the spectral calibration may shift is limited by the thermal inertia of the spectrometers and the rate at which the thermal environment of the spectrometer changes. The fastest change has a 100-minute period, corresponding to the spacecraft orbit. The spectral calibration is evaluated every six minutes, defined as a granule of data.

The “at launch” L1B V5 solved for Δy_0, ΔF and F_k and a mean(y_0^k), and reported the position of the focal plane as “spec_shift_upwell”, “ spec_shift_unc_upwell” in focal plane coordinates in units of micrometers (μm). The “spec_shift_unc” parameter is a flag with value 0 (good) and 1 (bad). The

grating model was used to calculate the corresponding 2378x1 "spectral_freq" array in wavenumber units. The "nominal_freq" is based on Δy_0=-13.5 μm for all 17 modules.

The L1B V8 includes a modified version of the "at launch" calibration for data continuity, called V8 M10 and a version that operates on the two halves of each module called V8 half-module. Both use the F_k derived in L1B V5 and specified in the grating model specification file (finalgm.mat), with $\Delta F=0$.

4.4. Algorithm

4.4.1. The V8 M10 Algorithm

This algorithm assumes that all 17 modules in the AIRS focal plane move together, that y_0^k for the seventeen modules in the focal plane is fixed and can be determined off-line and $\Delta F=0$. The spectral calibration is thus reduced to determining Δy_0 using the highest spectral contrast channels. These channels are on detector module M10 and the contrast is created by the CO_2 opacity. The spectral calibration finds the offset between each observed clear spectrum relative to the best matching reference spectrum uses a library of spectra precalculated using the SARTA Radiative Transfer Method (RTM) for a wide range of conditions, locations and CO_2. mixing ratios. Clear spectra in each granule are selected by comparing the surface skin temperature (SST) to the temperature expected based on climatology. The climatology was derived from the European Center for Medium Range Forecasting (ECMWF) based on 2005 through 2008 monthly averages, which are presented on a 1 degree lat/lon grid for the day and the night orbits. The SST is computed using two window channels: 1231.3 cm^{-1} (PGE#1291), and 1227.75 cm^{-1} (PGE#1284). The actual cloud filter looks at the absolute value of the difference between the computed SST and the climatology temperature. If the surface is frozen (ECMWF temperature less than 274), the SST's must agree with the climatology within 9.0 K. If it is land, the threshold is 4.5 K. If it is water, the threshold is 3.0 K. For each clear spectrum in a granule, the optimum reference spectrum is selected and the shift Δy_0 which achieves the peak correlation with the clear spectrum is recorded. The algorithm records the mean Δy_0 and the probable error of Δy_0 based on the ensemble of all clear spectra in the granule as specshift_y0 and specshift_y0_unc for each data granule. A specshift_ y0_unc =1 flags granules were the specshift_y0 did not pass a quality control filter.

4.4.2. The V8 half-module Algorithm

This algorithm, referred to as the halfmod algorithm, assumes that, while the seventeen detector modules are physically fixed in the focal plane, their effective positions, y_0^k , may move due to temperature gradient induced distortion of their separate optical trains, i.e. y_0^k and its uncertainty has to be determined independently for each detector module. To this end the spectra on the seventeen modules are split into 34 half_modules numbered 1 through 34, and the absolute value of the difference between y_0^k_odd and y_0^k_even is interpreted as a component of the measurement uncertainty. Table 4-1 defines the numbers, names, start and end wavenumbers, spectral contrast and sensitivity for a tropical temperature profile. We define the spectral contrast as the standard deviation of the difference between adjacent spectral samples of the spectrum. The higher the contrast, the more accurate the spectral calibration can potentially be. We define the sensitivity as the standard deviation of the brightness

temperature due to a one μm shift in the spectral calibration. The larger the sensitivity, the more important it is to have a stable the spectral calibration.

The algorithm uses a library of 7377 spectra calculated using a Line-by-Line RTM (kCARTA) for reference frequencies corresponding to y_o = -13.5 μm. The 7377 atmospheric states were selected by stratified surface temperature, latitude, solar zenith angle and scan angle sampling from one day (20110711) of ECMWF data (Ref. 18).

The algorithm identifies the 1215 of the 12150 spectra in a granule which are warmer than the 90th percentile of the brightness temperature in the 1231.3 cm^{-1} (PGE#1291) channel as clear and averages them into one "test spectrum". The test spectrum is then compared with a 50 principle component (PC) reconstruction. Channels which differ for the PC reconstruction by more than 1K, typically 24 of 2378 channels with NeDT>3K and 62 channels dead since launch, are replaced by their PC reconstructed brightness temperatures. The mean brightness temperature in each half-module is then compared to the corresponding brightness temperature in the reference spectra. For the subset of the reference spectra which agree with the test spectrum within 5K, typically hundreds of spectra. The algorithm then selects the reference spectrum with the highest correlation with the test spectrum. For this pair the algorithm saves the spectral contrast bttest_contrast, btref_best_contrast, the shift required for the reference spectrum to reach the peak correlation, y_o^k, and the value of the peak correlation, cor_peak.

Details: The algorithm finds the peak correlation between the best matching reference spectrum and the test spectrum in two steps. It defines a 21-point vector x1 between -11 and +11 μm in 1 μm steps. It then finds the rough peak of the correlation at x1max (using functions "spline" and "corr"). It then finds the fine location of the peak by fitting a parabola to x1 (using "polyfit") and by interpolating the parabola between xmax-1 and xmax+1 in 0.01 μm steps (using "polyval"). It returns the position of the peak as rrmax relative to the reference spectrum and the peak correlation as cor_peak. A rrmax value of +11 or -11 μm indicates that no peak position was found. If nbest=0, i.e. none of the reference spectra agreed with the observations in the modules within 5K, and sets rrmax=NaN. y_o^k *=rrmax-13.5μm*

After looping through the 34 half modules, y_o^k,is a 34-element array. In the L1B record it is referred to as spec_halfmod_shift_y0.

Table 4-1. Definition of the 34 half-modules.

Name	Boundaries [cm-1]	Element count	Contrast [K]	Sensitivity [K]
1 m1a	2618 2668	44	0.9	0.019
2 m1a	2570 2617	45	0.6	0.012
3 m2a	2490 2540	46	0.1	0.002
4 m2a	2442 2489	42	0.1	0.002
5 m1b	2372 2422	51	2.4	0.049
6 m1b	2326 2371	48	1.0	0.021
7 m2b	2211 2300	93	1.6	0.030
8 m2b	2120 2210	32	1.4	0.029
9 m4a	1577 1613	50	3.7	0.068
10 m4a	1540 1576	51	4.6	0.090
11 m4b	1493 1528	53	4.2	0.084
12 m4b	1460 1492	52	4.8	0.096
13 m3	1394 1443	85	5.1	0.109
14 m3	1338 1393	106	5.2	0.115
15 m4c	1321 1336	25	7.6	0.147
16 m4c	1284 1320	62	6.4	0.123
17 m4d	1255 1272	31	5.5	0.107
18 m4d	1217 1256	74	4.3	0.084
19 m5	1097 1136	74	2.8	0.050
20 m5	1056 1096	82	2.0	0.036
21 m6	1010 1040	67	1.8	0.034
22 m6	975 1009	81	1.0	0.020
23 m7	943 973	76	1.1	0.023
24 m7	974 1040	153	1.4	0.027
25 m8	876 900	72	1.5	0.034
26 m8	853 875	70	1.8	0.044
27 m9	810 851	105	1.6	0.029
28 m9	790 810	55	4.4	0.084
29 m10	743 760	53	8.8	0.177
30 m10	729 740	35	11.4	0.234
31 m11	722 728	20	11.2	0.231
32 m11	710 718	28	9.0	0.189
33 m12	670 682	47	7.0	0.159
34 m12	650 660	41	6.9	0.157

4.4.3. Spectral Calibration for one day.

There are two spectral calibration algorithms in L1B V8: One derived Δy_0 for module M10. In order to calculate the 2378x1 array spectral_freq we have to assume that y_0^k for the other 16 modules are given as offsets relative to M10. The halfmod calibration derives y_0^k, for k=34 half-modules. These have to be converted to the 17 modules using some algorithm. We first compare the to methods for M10, then we discuss an algorithm.

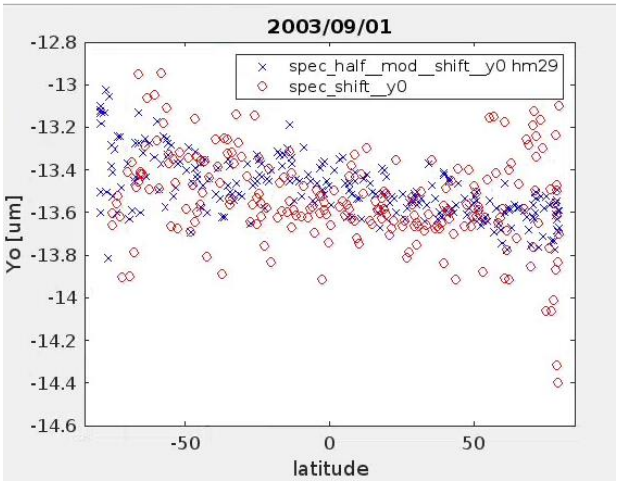

Figure 4-2. Overlay of spec_shift_y0 and half-module hm29 as function of latitude.

Figure 4-2 is a plot of spec_halfmod_shift_y0 for half-module hm29, the odd numbered side of M10, and spec_shift_y0 as function of granule mean latitude for a typical day, 2003/09/01. Both calibration methods show a small negative slope as function of latitude. At high latitudes both spectral calibrations become noisy. Averaging over all latitudes we find

M10 hm29 mean±stdev= -13.48 ± 0.14 µm (N=240)
Spec_shift_y0 mean±stdev= -13.53 ± 0.22 µm (N=220)

Where N is the number of valid solutions.

The M10 hm29 and spec_shift_y0 differ by 0.05µm. This is a small difference, but if one assumes that the Probable Error (PE) is given by stdev/√N, then PE=0.01 µm and the two solutions are statistically not consistent. However, one mean is based on 240 granules, while the other is for 220 modules.

By design, there can only be one Yo for each module, but since the observations are noisy, numerically we may well derive a mean1 with uncertainty1, and mean2 with uncertainty2. Ideally mean1+unc1 should overlap mean2-unc2. If they don't, then the uncertainties have been underestimated. The best estimate of the mean in that case is the inverse variance weighted mean, and the best estimate of the uncertainty is (mean1-mean2)/2+rss(uncertainty1, uncertainty2). The second column in Table 4-2. shows the results for the half-module averaged mean and uncertainties for all modules. For M10 mean±unc= -13.56 ± 0.17 µm. Now the two spectral calibration results agree from M10.

Inspection of Table 4-2 shows that the uncertainty for only four modules, M4b, M3, M4d and M10, is 0.2 µm or less. This should be expected, since these modules also have high spectral contrast (Table 4-1). Table 4-2 also shows that the spectral calibration for some modules does not return a solution for all 240 modules. Differences at the 0.5µm level were expected due to limitations of physically placing the arrays on the focal plane, For three modules, M6, M7 and M8, Yo differs by 1µm from M10. M6, M7 and M8 are low spectral contrast modules, which makes the spectral calibration difficult, but where a 1 µm shift produces a bias of less than 50 mK (Table 4-1). For many applications a spectral calibration within 1µm in focal plane coordinates, i.e. 1% of the SRF width, is acceptable. For these cases the daily mean of spec_shift_y0 should be used.

Table 4-2. Day/night averaged spectral calibration for 2003/09/01

name	Mean ± unc N All latitudes	LSQFIT Mean ± unc abs(lat)<60	LSQFit slope ± unc abs(lat)<60
1 m1a	-13.96 ± 0.58 202	-14.12 ± 0.26 153	-0.00115 ± 0.00203 153
3 m2a	NaN ± NaN 1	NaN ± NaN 81	NaN ± NaN 81
5 m1b	-13.35 ± 0.86 115	-15.15 ± 1.22 160	0.00271 ± 0.00091 160
7 m2b	-13.96 ± 0.85 170	-14.00 ± 0.53 162	0.00069 ± 0.00101 162
9 m4a	-13.92 ± 0.61 239	-13.89 ± 0.52 161	0.00017 ± 0.00048 161
11 m4b	-13.39 ± 0.13 240	-13.38 ± 0.01 161	-0.00014 ± 0.00009 161
13 m3	-13.10 ± 0.20 240	-13.12 ± 0.03 160	0.00006 ± 0.00023 160
15 m4c	-13.30 ± 0.19 240	-13.26 ± 0.09 160	0.00013 ± 0.00009 160
17 m4d	-13.17 ± 0.37 239	-13.17 ± 0.09 162	-0.00002 ± 0.00018 162
19 m5	-13.47 ± 0.48 226	-13.31 ± 0.24 154	-0.00002 ± 0.00008 154
21 m6	-12.50 ± 0.26 177	-12.46 ± 0.16 160	0.00003 ± 0.00071 160
23 m7	-12.61 ± 0.61 209	-12.49 ± 0.30 157	0.00034 ± 0.00083 157
25 m8	-12.38 ± 0.38 46	-12.55 ± 0.70 149	-0.00123 ± 0.00273 149
27 m9	-13.34 ± 0.47 201	-13.34 ± 0.20 159	-0.00060 ± 0.00129 159
29 m10	-13.56 ± 0.17 240	-13.54 ± 0.06 161	0.00003 ± 0.00001 161
31 m11	-13.87 ± 0.51 238	-13.83 ± 0.43 158	-0.00013 ± 0.00012 158
33 m12	-13.88 ± 0.33 214	-13.83 ± 0.21 157	0.00036 ± 0.00006 157

For a more accurate daily spectral calibration, the calibration could be based on linear least squares fit to the results from the 162 granules between latitude 60S and 60N. Results are shown in Table 4-2. The offset of the least squares fit (LSQFIT) agrees with the mean for all latitudes. The slope is very small and not reliable based on one day of data. We recommend that the spectral calibration based on one day of data should use the noise weighted mean from all granules, and no slope. A more precise spectral calibration could be derived using a longer time period, which would distinguish between day and night orbits and a use a slope. This will be addressed for L1C V8.

A bias in the spectral calibration is relevant for real-time applications only if it exceeds the absolute radiometric calibration accuracy. If we take 0.1 K as the absolute radiometric calibration uncertainty, then only 5 of the 17 modules require a spectra calibration of better

Table 4-3. Day/night averaged relative spectral calibration for 2003/09/01

name	All latitudes	N
1 m1a	mean±PE -13.926± 0.037 N=	196
3 m2a	mean±PE -13.365± 0.030 N=	118
5 m1b	mean±PE -13.685± 0.076 N=	90
7 m2b	mean±PE -13.722± 0.038 N=	221
9 m4a	mean±PE -13.805± 0.011 N=	240
11 m4b	mean±PE -13.386± 0.007 N=	240
13 m3	mean±PE -13.096± 0.014 N=	240
15 m4c	mean±PE -13.280± 0.016 N=	238
17 m4d	mean±PE -13.171± 0.013 N=	240
19 m5	mean±PE -13.534± 0.027 N=	218
21 m6	mean±PE -12.435± 0.015 N=	208
23 m7	mean±PE -12.647± 0.024 N=	217
25 m8	mean±PE -12.430± 0.022 N=	113
27 m9	mean±PE -13.249± 0.023 N=	223
29 m10	mean±PE -13.569± 0.008 N=	240
31 m11	mean±PE -13.733± 0.013 N=	238
33 m12	mean±PE -13.899± 0.014 N=	216

than 1 μm. Random errors in the spectral calibration cancel for climate applications. However, a shift of the spectral calibration would create trend artifacts, which, if not detected, would be misinterpreted as climate trends. A detection of a trend in the spectral calibration is ultimately limited by the noise in the daily measurements. Table 4-3. shows the daily mean and PE for the 17 modules. For example, for M10 the PE based on daily measurements is 0.008 μm, which corresponds to a radiometric shift of (average of hm29 and hm30 from Table 4-1) (0.177+0.234)/2 K/μm * 0.008 μm = 1.6 mK. The stability of AIRS has been estimated as 2 mK/year or less for the past 20 years based on atmospheric window channels where the spectral calibration is uncritical. A 2 mK/year trend in M10 would be created by a trend in Yo of 0.003 μm/year. From Table 4-3 we can see that the PE for M10 is only 0.008μm with one day of data. For all but two of the SW modules the PE is less than 0.04μm. We conclude that the stability of the AIRS spectral calibration can be monitored using the daily L1B spectral calibration with sufficient accuracy that, when corrected in L1C, the residual trends will be less than the equivalent of 2 mK/yr.

5. Spatial Calibration

The AIRS Level 1B radiances are computed from the signals observed from the instrument, space, and the on-board calibrators. The computation does not include information about the spatial dependence of the instrument or scene. The actual radiance observed by AIRS will depend on the convolution of the AIRS point spread response function (PSF) and the underlying spatially variant scene radiance. For uniform scenes, or when taking large ensemble averages, the radiances are unaffected by the AIRS PSFs. However, when the scene is non homogenous, most notable on the edges of cold clouds, the PSFs can produce shifts in the spectra for those channels whose PSFs differ significantly from the average of all the channels. These scenes are flagged in the Level 1B (delta_rad_inhomo_sw, and delta_rad_inhomo_lw) . More information on the impact of scene spatial inhomogeneity on the AIRS radiances, and a potential technique using MODIS and the AIRS PSFs to correct for variability amongst the channels is given in Ref. 19. The Level 1C product detects these conditions and replaces affected channels with their PC reconstruction. Both methods work equally well. For more information please see the Level 1C data product user guide.

A common latitude and longitude is provided in the AIRS level 1B for all spectral channels. The geolocation is computed using a model of the AIRS scan mirror, alignment of the instrument to the spacecraft and the pointing of the Aqua satellite. The algorithm used for the Level 1B infrared radiance product is the same as that used in the Vis/NIR except only the center of the field is used and is documented in the AIRS Vis/NIR Geolocation algorithm. Pointing accuracy for the AIRS has been shown to be better than 0.1 degree (about 1km at nadir). More information can be found in the AIRS Level 1B test report.

6. References

1. Morse, P, J. Bates, C. Miller, M. Chahine, F. O'Callaghan, H. H. Aumann and A. Karnik, "Development and Test of the Atmospheric Infrared Sounder (AIRS) for the NASA Earth Observing System (EOS)", Proc. SPIE 3870-53, 1999. https://doi.org/10.1117/12.373196
2. AIRS Functional Requirements Document, JPL Internal Document D-8236, Rev. 1., Oct. 1992.
3. AIRS Visible and Infrared In-Flight Calibration Plan, Version 3.0, June 2002, JPL D-118816
4. M.T. Chahine, et al., AIRS Team Science Validation Plan, Core Products, JPL D-16822, Version 2.1.1, June 5, 2000, https://eospso.gsfc.nasa.gov/sites/default/files/atbd/AIRSValP2doc.pdf
5. Pagano, T. et al., "AIRS Version 8 Level 1B Test Report", May 22, 2024, https://disc.gsfc.nasa.gov/information/documents?title=AIRS%20Documentation
6. Aumann, H.H. , M.T. Chahine, C. Gautier, M. Goldberg, E. Kalnay, L. McMillin, H. Revercomb, P.W. Rosenkranz , W. L. Smith , D. H. Staelin, L. Strow and J. Susskind, "AIRS/AMSU/HSB on the Aqua Mission: Design, Science Objectives, Data Products and Processing Systems", IEEE Transactions on Geoscience and Remote Sensing, Feb 2003, Vol.41.2. pp. 253-264. https://ieeexplore.ieee.org/document/1196043
7. Pagano, T.S., H. Aumann, S. Broberg, C. Canas, E. Manning, K. Overoye, R. Wilson, "SI-Traceability and Measurement Uncertainty of the Atmospheric Infrared Sounder Version 5 Level 1B Radiances", *Remote Sens.* 2020, *12*, 1338; https://doi.org/10.3390/rs12081338
8. Pagano T.S., H.H. Aumann, L. Strow, "Pre-Launch Performance Characteristics of the Atmospheric Infrared Sounder", Proc. SPIE 4169-41, September 2000. https://doi.org/10.1117/12.417132
9. Pagano, T.S, H. H. Aumann, D. Hagan and Ken Overoye, "Prelaunch and In-Flight Radiometric Calibration of the Atmospheric Infrared Sounder (AIRS)", (2003) IEEE Transactions on Geoscience and Remote Sensing, Vol.41.2, pp. 265-273. https://doi.org/10.1109/TGRS.2002.808324
10. Pagano, T.S. et al., "Updates to the Radiometric Calibration of the Atmospheric Infrared Sounder (AIRS)", Proc. SPIE 12685-19, San Diego, Ca (2023), http://dx.doi.org/10.1117/12.2676416
11. Aumann, H.H. et al., "Evaluating the Absolute Calibration Accuracy and Stability of AIRS using the CMC SST", Remote Sens. 2020, 12(17), 2743; https://doi.org/10.3390/rs12172743
12. Tobin, David, Henry E. Revercomb, Chris Moller, Robert O. Knuteson, Fred. A. Best, William. L. Smith,Paul Van Delst, Daniel D. LaPorte, Scott D. Ellington, Mark W. Werner, Ralph G. Dedecker, Ray K. Garcia, Nick N. Cigonovich, H. Benjamin Howell, Steven Dutcher and Joe K. Taylor (2004), "Validation of Atmospheric Infrared Sounder (AIRS) Spectral Radiances with the Scanning High-resolution Interferometer Sounder (S-HIS) Aircraft Instrument", Proc-SPIE, 5571, https://doi.org/10.1117/12.566060, 383-392.
13. Walden, V. P., W. L. Roth, R. S. Stone, and B. Halter (2006), Radiometric validation of the Atmospheric Infrared Sounder over the Antarctic Plateau, J. Geophys. Res., 111, D09S03, https://doi.org/10.1029/2005JD006357
14. Aumann, H. H., Broberg, S., Manning, E., & Pagano, T. (2019). Radiometric Stability Validation of 17 Years of AIRS Data Using Sea Surface Temperatures. *Geophysical Research Letters*, 46. https://doi.org/10.1029/2019GL085098
15. Strow, L. L. and S. DeSouza-Machado (2020) "Establishment of AIRS climate-level radiometric stability using radiance anomaly retrievals of minor gases and sea surface temperature" Atmos.Meas.Tech, 13, 4619-4644, 2020 https://doi.org/10.5194/amt-13-4619-2020

16. Strow, L. L., Scott E. Hannon, Margeret Weiler, Kenneth Overoye, Steven L. Gaiser and Hartmut H. Aumann, "Prelaunch Spectral Calibration of the Atmospheric Infrared Sounder (AIRS)", IEEE Transactions on Geoscience and Remote Sensing, Feb 2003, V.41,#2, 274-286, https://doi.org/10.1109/TGRS.2002.808245
17. Gaiser, Steve L., Hartmut H. Aumann, L. Larrabee Strow, Scott Hannon and Margaret Weiler, "In-Flight Spectral Calibration of the Atmospheric Infrared Sounder", IEEE Transactions on Geoscience and Remote Sensing, Feb 2003, V.41,#2, 287-297, https://doi.org/10.1109/TGRS.2003.809708
18. Aumann, H. H., Chen, X., Fishbein, E., Geer, A., Havemann, S.,Huang, X., Liu, X., Liuzzi, G., DeSouza-Machado, S., Manning, E. M., Masiello, G., Matricardi, M., Moradi, I., Natraj, V., Serio,C., Strow, L., Vidot, J., Wilson, R. C., Wu, W., Yang, Q., and Yung, Y. L. (2018), Evaluation of Radiative Transfer Models with Clouds, J. Geophys. Res.-Atmos., 123, 6142-6157. https://doi.org/10.1029/2017JD028063
19. T.S. Pagano, H. Aumann, D. Elliott,, E. Manning, "Improving AIRS radiance spectra in high contrast scenes using MODIS', Proc. SPIE 9607-19, San Diego, CA (2015). https://doi.org/10.1117/12.2188311

7. Dictionary of Abbreviations

ADC	Analog-to-Digital Converter
AIRS	Atmospheric Infrared Sounder
AMA	Actuator Mirror Assembly
AMSU	Advanced Microwave Sounding Unit
ATBD	Algorithm Theoretical Basis Document
ATCF	AIRS Test and Calibration Facility
CSV	Cold Space View
CMCSST	Canadian Meteorological Center Sea Surface Temperature
DCR	DC Restore (of the electronics)
DN	Data Number
ECMWF	European Center for Medium Range Forecasting
EM	Engineering Model
EOS	Earth Observing System
FOV	Field of View (projected on the ground pertaining to one dwell time)
FRD	Functional Requirements Document
FWHM	Full-Width Half-Maximum
GES DISC	Goddard Earth Sciences Data and Information Services Center
GSFC	Goddard Space Flight Center
HgCdTe	Mercury-Cadmium Telluride
HSB	Humidity Sounder for Brazil
IFOV	Instantaneous Field of View. Smaller or equal to the FOV.
IR	Infrared
JPL	Jet Propulsion Laboratory

LABB	Large Aperture Blackbody
LSQFIT	Linear Least Squares Fit
MIV	Moon in View
MODIS	Moderate Resolution Imaging Spectroradiometer (on EOS Terra and Aqua)
MSU	Microwave Sounding Unit
NASA	National Aeronautics and Space Administration
NEdT	Noise Equivalent Delta Temperature
NEN	Noise Equivalent Radiance
NESDIS	National Environmental Satellite, Data, and Information Service
NIR	Near Infrared (between 1 and 3 microns)
NIST	National Institute of Standards and Technology
NOAA	National Oceanic and Atmospheric Administration
OBC	On-Board Radiometric Calibrator
OBS	On-Board Spectral reference source
PC	Photoconductive Detector
PE	Probable Error of the mean
PFM	Proto Flight Model
PGE	Product Generation Executive
PRT	Platinum Resistance Thermometer
PV	Photovoltaic Detector
QA	(Data) Quality Assessment
QC	Quality Control
RTA	Radiative Transfer Algorithm based on a RTM
RTG-SST	Real-Time Global Sea Surface Temperature

RTM	Radiative Transfer Model, used by the RTA
SHIS	Scanning High-resolution Interferometer Sounder
SRF	Spectral Response Function
SST	Sea Surface Temperature
SVBB	Space View Blackbody
SVS	Space View Source
SW	Short-Wave
TVAC	Thermal Vacuum Chamber
T/V	Thermal Vacuum
VIS	Visible wavelength